POLITECNICO DI TORINO

Department of Energy Engineering

Master of Science program
in Energy and Nuclear engineering

Master Thesis

Kinetic modeling of CO_2 splitting reactions using perovskites in chemical looping for syngas production

Mentors

prof. Eng. Massimo Santarelli

.....

Eng. Domenico Ferrero

.....

Candidate
Federico Russo

.....

March 2021

A tutte le persone che hanno subito quest'insopportabile 2020.

Che l'innovazione scientifica continui ad essere il luminoso faro nel buio oceano del futuro.

To all the people, who suffered this unbearable 2020.

Let the scientific innovation keep being the shining beacon in the dark ocean of the future.

Abstract (italian version, versione italiana)

Questo lavoro, inserito in un progetto di collaborazione internazionale (Politecnico di Torino, Università di Udine e Massachusetts Institute of Technology), ha l'ambizioso intento di suggerire una parziale soluzione per il raggiungimento di alcuni dei Sustainable Development Goals, forniti dalle Nazioni Unite (nello specifico, i numeri 7, 9, 11, 13)[1].

L'obiettivo generale si concretizza in quello più specifico: uno studio cinetico e quantitativo, della produzione di monossido di carbonio, usando la perovskite SFNM ($Sr_2FeNi_{0,4}Mo_{0,6}O_{6-\delta}$), tramite un ciclo chimico (*chemical looping*) che lavora dividendo l'anidride carbonica. Proprio nell'utilizzo di questo materiale, nella propria applicazione, risiede la novità della presente ricerca. Lo studio è basato su un'analisi Termogravimetrica del materiale, supportata da un modello cinetico della reazione con la CO_2 e da un modello della sua applicazione in un reattore.

La decarbonizzazione può essere favorita solo se le infrastrutture collegate alle risorse rinnovabili verranno potenziate. Questo percorso deve essere perseguito per ottenere uno sviluppo sostenibile.

Questo breve contesto è il tema principale sviluppato nel primo capitolo della presente. Inoltre, verranno forniti alcuni concetti preliminari, collegati allo *splitting* dell'acqua e del diossido di carbonio, processato tramite *chemical looping*.

Nello stesso capitolo, viene fornita una rassegna delle principali soluzioni presenti in letteratura, utili al confronto con la novità introdotta dalla presente ricerca, congiuntamente con, in ampia scala, i lavori ad essa correlata.

Il capitolo 2 di questa ricerca rappresenta un passaggio preliminare per la stima delle caratteristiche del sistema. Infatti, l'Analisi Termogravimetrica è essenziale per ogni studio, che ha, come obbiettivo, la stima delle proprietà di un nuovo materiale (SFNM). Tramite quest'indagine, verranno confermate la durabilità e la ciclabilità della perovskite in questione.

Il cuore della dissertazione si apre nella sezione numero 3; in questa, basandosi sui risultati forniti dal capitolo precedente, viene predisposta una prima valutazione cinetica. L'investigazione è condotta usando un classico metodo di fittaggio, il quale fornisce il miglior modello, per simulare le reazioni durante l'ossidazione del materiale studiato. La curva più adatta deve essere aderente alla soluzione teorica, offerta dalla propria teoria cinetica delle reazioni. Su queste premesse, si fonda una valutazione dei parametri caratteristici (energia di attivazione e fattore di frequenza), per una stima del tasso di reazione; usando un *fitting* iterativo.

Pur essendo fornita una prima valutazione cinetica, le prestazioni del materiale devono essere estrapolate a livello del reattore, con uno studio più strutturato, usando un software di simulazione multifisica.

Nel capitolo 4, è stato elaborato uno studio basato sulle reali caratteristiche geometriche e dei materiali, che definiscono il microreattore; incubatore delle reazioni citate. La linea seguita è rappresentata da un'unione di diverse fisiche, legate alla fluidodinamica ed alla chimica.

Nel capitolo 5, è sviluppata la fase sperimentale finale, con un'empirica validazione dei modelli ottenuti precedentemente.

L'analisi conclusiva è inserita nel capitolo 6, commentando i risultati ottenuti e sottolineando la mancata concordanza tra il modello sviluppato ed i dati misurati nel microreattore.
La discussione su quest'aspetto, congiuntamente con le possibili prospettive per raggiungere i risultati prefissati, in lavori futuri, chiude questa tesi di laurea magistrale.

Index

Figures index

Equations Index

Tables Index

List of symbols and acronyms

E_a	*Activation Energy* $[J]$
AIC	*Akaike Information Criterion*
Ar	*Argon*
d_p	*Average Diameter of grains* $[m]$
AE	*Avrami-Erofeev*
CCS	*Carbon Capture & Sequestration*
CO_2	*Carbon Dioxide*
CDS	*Carbon Dioxide Splitting*
CO	*Carbon Monoxide*
P_i	*Chemical Product of the i-th species*
R_i	*Chemical Reagent of the i-th species*
L_{co_2}	*CO_2 reactor length* $[m]$
R^2	*Coefficient of determination* $[-]$
C	*Concentration of chemical species* $\left[mol/_{m^3}\right]$
c_i	*Concentration of the i^{th} species* $[mol]$
R_i	*Concentration rate of the i^{th} species* $\left[\frac{mol}{s}\right]$
k(T)	*Constant rate* $\left[1/_s\right]$
f(α)	*Conversion function in the differential form* $[-]$
g(α)	*Conversion function in the integral form* $[-]$
ρ	*Density* $\left[\frac{kg}{m^3}\right]$
O_2	*Diatomic Oxygen*
DAE	*Differential Algebraic Equation*
dt	*Differential timestep range* $[s]$
D_i^f	*Diffusion coefficient* $[m^2/s]$
$\vec{J}_i$	*Diffusive Mass flow rate per unit Area* $\left[\frac{kg}{m^2 s}\right]$
EDX	*Energy dispersive X-ray*
FESEM	*Field Emission Scanning Electron Microscopy*
μ	*Fluid Viscosity* $[Pa\ s]$
β	*Forchheimer drag coefficient* $\left[\frac{1}{m}\right]$
δ	*Fraction of reducible cations unreacted*

k_0	*Frequency/pre-exponential factor* $\left[{}^{1}/_{s}\right]$
$GHSV$	*Gas Hourly Space Velocity* $\left[{}^{Nm^3}/_{h\ m}\right]$
MeO	*Generic Metal Oxide*
GHG	*Greenhouse Gases*
H_2	*Hydrogen*
$\vec{l}$	*Identity vector* $[-]$
m_0	*Initial mass* $[kg]$
n_0	*Initial mole* $[mol]$
IEA	*International Energy Agency*
$FeNi$	*Iron-Nickel alloy*
LSF731	$La_xSr_{1-x}FeO_3$ *perovskite*
$m(t)$	*Mass at the timestep t* $[kg]$
x_i	*Mass fraction of the* i^{th} *species* $[-]$
MSE	*Mean squared error* $[-]$
CH_4	*Methane*
MIT	*Michigan Institute of Technology*
ω_i	*Molar fraction of the* i^{th} *species* $[-]$
R	*Molar gas constant* $\left[{}^{J}/_{K\ mol}\right]$
MW_i	*Molar Weight of the* i^{th} *species* $[-]$
Mo	*Molybdenum*
N_2O	*Nitrous Dioxide*
α	*Normalized mass variation* $[-]$
ODE	*Ordinary Differential Equation*
Ox	*Oxidation*
m_{end}	*Oxidized final mass*
O	*Oxygen*
κ	*Permeability* $[m^2]$
ε	*Porosity* $[-]$
p	*Pressure* $[Pa]$
r	*Reaction rate* $\left[{}^{mol}/_{s\ m^3}\right]$
Red	*Reduction*
SEM	*Scanning Electron Microscope*
SFNM	$Sr_2FeNi_{0,4}Mo_{0,6}O_{6-\delta}$ *perovskite*

D_{SFNM}	*SFNM reactor Diameter* $[m]$
L_{SFNM}	*SFNM reactor length* $[m]$
Vol_{SFNM}	*SFNM Volume* $[m^3]$
Q_{sv}	*Standard Flow Rate* $[m^3/s]$
m_{CO}	*Stoichiometric CO mass production* $[kg]$
ν	*Stoichiometric coefficient*
ν_i	*Stoichiometric coefficient of the* i^{th} *species* $[-]$
Sr	*Strontium*
$SrCO_3$	*Strontium Carbonate*
$SrMoO_4$	*Strontium Molybdate*
SDG	*Sustainable Development Goals*
T	*Temperature* $[K]$
TPO	*Temperature-Programmed Oxidation*
TPR	*Temperature-Programmed Reduction*
TGA	*Thermogravimetric analysis*
t	*Time* $[s]$
τ_g	*Tortuosity* $[-]$
UniUd	*Università degli studi di Udine*
$\vec{u}$	*Velocity* $\left[\frac{m}{s}\right]$
Vol	*Volume* $[m^3]$
F	*Volume Force* $[N/m^3]$
H_2O	*Water*
WS	*Water Splitting*
WEO	*World Energy Outlook*
XRD	*X-Ray Diffraction*

Abstract

This work, inserted in an international collaboration project (Politecnico di Torino, Università di Udine and Massachusetts Institute of Technology), has the ambitious intent to suggest a partial solution to face the fulfillment of certain Sustainable Development Goals (SDG) provided by United Nations (more specifically, numbers 7, 9, 11, 13)[1].

The general purpose becomes realized in the specific one: the kinetic and quantitative estimation of the carbon monoxide production from carbon dioxide using a SFNM ($Sr_2FeNi_{0,4}Mo_{0,6}O_{6-\delta}$) perovskite through a chemical looping process. The innovation of this study lies in the investigation of the use of this material for this specific application. The study is based on the Thermogravimetric Analysis of the material to support the development of a kinetic model of the reaction with CO_2 and in the modeling of the application in a reactor.

Decarbonization could be accomplished only if renewable sources facilities will be enhanced. Stocking fuels for electrochemical cells and syngas, to save the unused renewable energy, has interesting perspectives. This pathway has to be followed in order to achieve an ecological development.

This brief context is the main theme explained in the first chapter of the present work. In addition, some introductory concepts, related to chemical looping for water and carbon dioxide splitting will be provided. In the same section, it will be inserted a review of the main solutions existing in literature, useful for comparing with the innovation introduced in the actual research, jointly with, in a large-scale, all works to it correlated.

The chapter 2 of this work stands for the preparatory step for estimation of the system features. In fact, the Thermogravimetric Analysis is essential for any study which handles properties estimation of a new material. Through this survey, the durability and the cycling of the perovskite has to be confirmed.

The core of the dissertation is opened in section 3; in this, basing on results provided by the previous chapter, a first kinetic evaluation is provided. The investigation is carried out using a classical fitting method, which supplies the best model to simulate reactions during oxidation of the studied material. The suitable curve has to be adherent to the theoretical solution, offered by the kinetic reactions theory. On these premises, an evaluation of the characteristic parameters (activation energy and frequency factor) for the rate of reaction estimation can be done using an iterative fitting.

Although a first kinetic evaluation is provided, the material performance has to be extrapolated to reactor level with a more well-structured analysis, using a multiphysics simulation software. In chapter 4, a model based on real geometrical and material features of a microreactor where the material will be tested has been developed. The outline is represented by a union of several Physics, concerning fluid dynamics and chemical reactions.

In the chapter 5, the final experimental phase is carried out and an empirical validation of the models previously developed is accomplished.

The summary analysis is performed in the chapter 6, commenting the results obtained, underlying the lack of agreement between the model developed and the measured data in microreactor. The discussion on this aspect, together with the feasible perspectives to reach results in future works, close this master thesis.

1. Introduction

In this opening section of the work, to achieve the full comprehension of the paper, some preliminary concepts will be provided.

After a brief motivational environmental framework, quite compulsory, given the always growing awareness for the theme; it has been inserted an essential explanation about chemical looping for water and carbon dioxide splitting.

Later, it will be explained the innovative material for which the study has been panned and some generic explanations, of the work road map, will be furnished.

To conclude, an exploration on existing review is developed, to understand what other authors researched in the near-past.

1.1. Overall framework

Nowadays, the energy panorama is strictly restrained by several factors.

A sustainable development will be possible only if hydrogen-based energy systems (and consequentially the ones using syngas) will begin spreading in a huge way.

This scenario is recommended by the International Energy Agency (IEA), through the World Energy Outlook (WEO) an essential, free-standing source for audience dealing in energy area.

This ecological pathway will become reality, only when renewable systems can deal with the "storage issue". In this point of view, the hydrogen and polygeneration vectors cover an inescapable role, providing facilities towards an eco-development.

Evidently, easy solutions for complicated problems are always trivial and fallacious. The energy world has to fight against several systemic disease, as: the increasing energy demands, especially from emerging countries, complexity linked to the energy markets, economic difficulties, for the innovative technologies, large scale taking-up.

These considerations validate the importance for the hydrogen and syngas diffusion, to face problems through solutions, and explain the will of expounding on this work.

As cited in the abstract of this research, the main aim of works developed in this historical phase should be the fulfillment of the Sustainable Development Goals (SDG) provided by United Nations.

The proper numbers 7, 9, 11, 13).

The main purpose of this work the kinetic and quantitative estimation of the hydrogen and carbon monoxide production using a SFNM ($Sr_2FeNi_{0,4}Mo_{0,6}O_{6-\delta}$) perovskite, working in a chemical looping, which splits water and carbon dioxide. Precisely the practice of this material, in the own application, lie the innovation of this study.

Decarbonization could be accomplished only if renewable sources facilities will be enhanced. This aspect is strongly highlighted in the international work: Tracking SDG 7, The Energy Progress Report[2]. Stocking fuels for electrochemical cells and syngas, to save the unused renewable energy, has interesting perspectives, from the above cited work, the orders of magnitudes are provided, they are near 11 EJ of global energy demand by 2030 (among these, near the 30% will be from renewable sources, almost doubling in 2050); these values exclude the geothermal and solar thermal sources, which have a huge role in the future.

Hydrogen and secondary fuels, produced using energy surplus, have a key role in the purpose cited. These options can be considered in the viewpoint of the environmental impact decrease in several fields, as the automotive, the aviation, the naval sector and the industrial one.

Green fuels are interesting in the "Transforming Energy Scenario", above-cited document.

The likely energy supply for renewable sources is estimated around 3.2 EJ, for the next ten years, near a third of the whole energy demand, doubling in the 2050.

For this perspective acquirement, the global commitment has to be increased, although investments are increased, in the last years, the necessity to help the renewable sector, to make it competing with the fossil industry, covers an always more predominant weightiness.

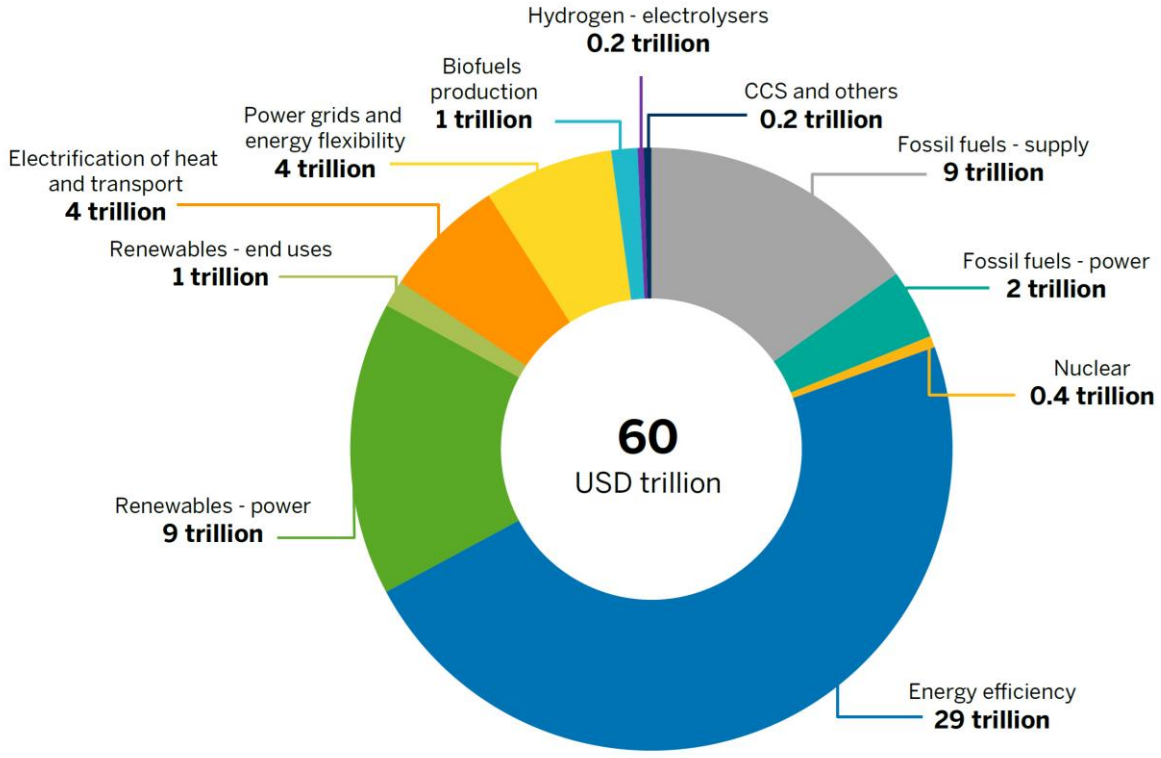

Source: IRENA 2020d.
CCS = carbon capture and storage.

Figure 1 - Investments in energy sector for the Transforming Energy Scenario until 2030.

In a parallel view, the carbon capture sequestration (CCS) is inserted.

The theme of the CCS is always more growing, in interest speaking, this care is related to the increasing of the greenhouse effect, enhanced by excessive anthropological processes, which are releasing the huge amount of greenhouse gases (GHG) in the atmosphere.

From main GHG, the most impacting are methane (CH_4), nitrous dioxide (N_2O), caused by the agriculture-farmer sector and the overcited carbon dioxide (CO_2). From these three, the last one, produced, in a synthetic way, as waste from power generation and transportation, is the focus of this recap.

Also if it is commonplace, the CO_2 presence in atmosphere is not a significant problem, in fact, as it is well known, it is produced naturally through several biological processes. The carbon dioxide production becomes an issue, in terms of global warming potential, when its manufacturing is sizeable, in a huge amount; in order to its high atmospheric residential time.

The production of CO_2 is quantified in the order of 33 Gt in the 2019, as reported by the International Energy Agency (IEA)[3].

From the same source, the growing trend of the CO_2 generated in the world for each year is provided in the *Fig. 2*:

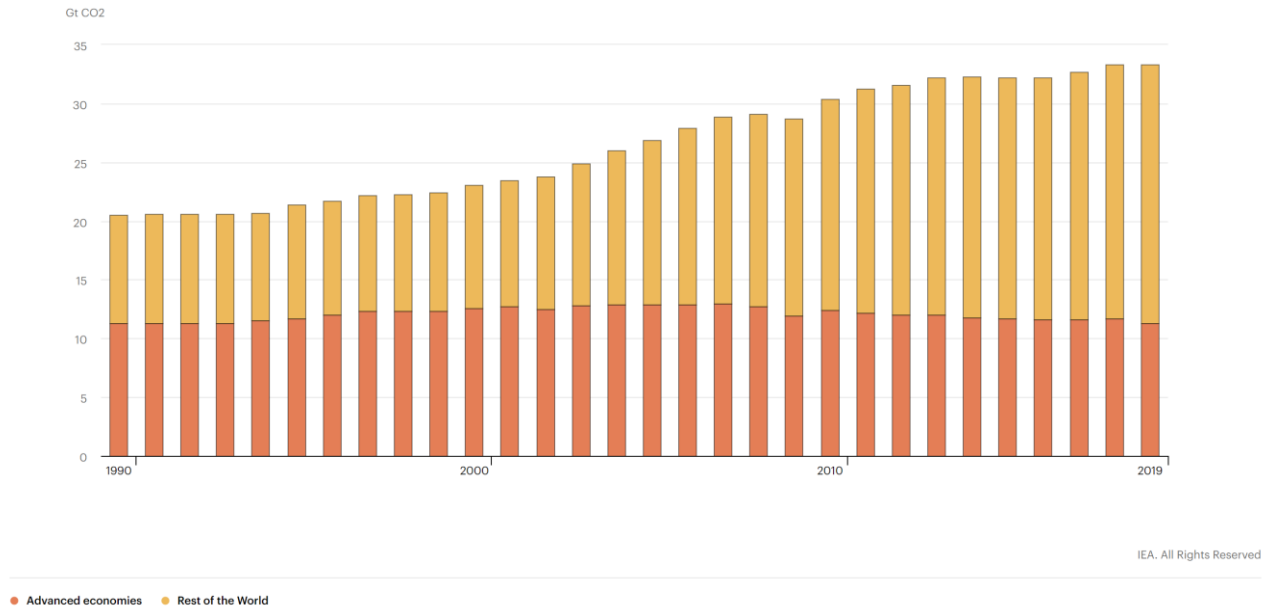

Figure 2 - CO2 emissions in 1990-2019

The impact of the always growing carbon dioxide fabrication has to be stopped, because of the incapability of the environment to absorb the surplus.

The only way to reduce the increasing rate of CO_2 yield is represented by the whole switch from fossil fuels technologies to the renewable one.

While the transition is implemented, CCS technologies represent an *interim* solution to decarbonized fossil fuel supplied plants.

Carbon capture & sequestration can be used in advanced polygeneration plants to mitigate the carbon impact of power generation and, potentially, manipulate the CO_2 sequestrated to make chemicals, giving birth to a second product, halving the impact of that carbon stream.

It is necessary underlying that, in the case of analysis, the carbon anhydride is not captured, but rather reused. In this path, the carbon capture & utilization, CO_2 is not stored, but exploited to produce chemicals (in this case carbon oxide, CO), which will be used to produce some useful effect (the use of the gas in an electrochemical way). The stream re-used and not only released in atmosphere let the double exploitation of it, halving the environmental impact.

1.2. Chemical looping

As reported[4] by M. Portarapillo et al. Using convenient materials, oxygen-carrier, CO_2 (in the Carbon Dioxide Splitting, CDS) and H_2O (in the Water Splitting, WS) can be used to reduce and oxidize, producing syngas, composed, mainly, by CO and H_2. According to the following reactions:

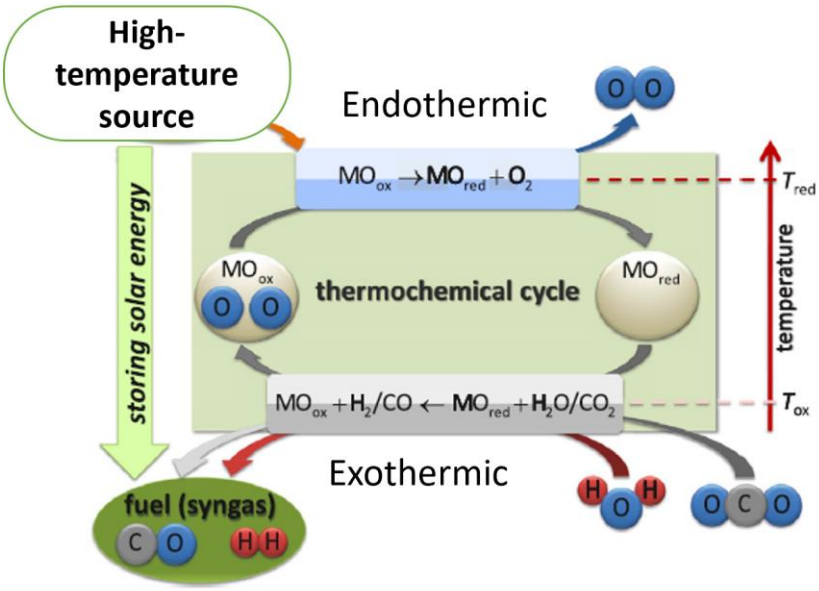

Figure 3: Generic Chemical looping for Syngas production

Reduction

CDS $$MeO_{Red} + CO_2 \rightarrow MeO_{Ox} + CO + Heat$$

WS $$MeO_{Red} + H_2O \rightarrow MeO_{Ox} + H_2 + Heat$$

Oxidation $$MeO_{Ox} + Heat \rightarrow MeO_{red} + \frac{1}{2} O_2$$

Equation 1: Chemical reactions for H_2O/CO_2 splitting.

Among the wide range of materials, if the Metal (Me) reported above is represented by Cerium, the oxygen carrier becomes the Cerium(IV) Oxide, also known as: Ceria. This choice provides a Non-Volatile cycle.

Throughout the several aspects, which curbs the proliferation of this technology there are: the high reduction temperature and the low oxidation kinetics. In this project, an alternative material is proposed for Ceria, looking over a kinetic model to estimate the velocity of reactions.
A thermogravimetric balance is used to analyzed the CO_2 splitting behavior, then, a microreactor analyses is implemented to investigate H_2O splitting feature.

1.3. The perovskite

The analysis, developed in this work, is based on a previous paper written by Università di Udine [5]
In the study, It is characterized a double perovskite oxide, composed by Strontium, Iron, Nickel and Molybdenum, according to the chemical formula: $Sr_2FeNi_{0,4}Mo_{0,6}O_{6-\delta}$.
One of the interesting feature of this material is related on its capability to grow, throughout the Hydrogen reducing, giving birth to an exsolution evolution, with the consequential appearance of spread Ni-Fe nanoparticles on the perovskite outer layer that enhance the catalytic activity of the SFNM surface.
Further to this, more inherent to the theme treated in the present, this perovskite shows a good stability with common electrolyte, in severe thermal conditions, guaranteeing the absence of derived aggregates. In addition, it has a discrete electronic and ionic conductivity, but above all, it is worthy of mention the excellent capability to conduct and remain stable in oxidizing and reducing environment.

1.4. Layout of the work

The objective of this work is to perform an analysis evaluating the perovskite $Sr_2FeNi_{0,4}Mo_{0,6}O_{6-\delta}$ performance, so if it can split CO_2 in a qualitative and quantitative evaluation.

The choice, of this material, is made for keeping lower the reduction temperature, abating drastically the fraction of reducible cations unreacted (δ), properly given by the working temperature lower than the one required.

This considerations are made in function of the temperature at which the process takes place; and in function of the partial pressure of the CO_2.

Through testing, it has been evaluated at different conditions: the quality of syngas produced, CO_2 reactions with the material and if the reaction is reversible to cycle it. Considering the innovation of this material, the lack of characterization for the material requires different testing conditions.

In the microreactors, high temperature feasible conditions have been simulated, neglecting fluid dynamic considerations, in first approximation, the Thermogravimetric analysis (TGA) has performed. This choice allows to save a huge amount of testing material, in fact, around 10 g of pulverized perovskite are necessary, rather than hundreds, which would be needed to develop a more detailed fluid dynamic analysis. This study is extended in the chapter two of the present work.

Later, to simulate microreactors condition more realistically, time has been reduced, always working at 900°C in reduction, and 500°C in oxidation (with CO_2). This TGA study is necessary to acquire the kinetic data.

From this experience, empirical data about mass variation and gas information are furnished; crossing these two empirical values, it is possible verifying, quantitatively, if the hydrogen consumption, during reduction, (and the CO production during oxidation) is consistently compared to the differential weight drop measured.

Knowing the exact value of hydrogen consumption or CO production, the variation of concentration in time can be calculated, obtaining the velocity of the reaction. In chapter three, the analysis will be focused on the kinetic considerations. In this step, the kinetic model fitting, on the TGA data, is acquired.

The simulation in the microreactor is implemented, using the Computational Fluid-dynamics, on the founded kinetics.

In the final stage, the results will be validated on a real microreactor.

1.5. Literature review

In literature, several studies have been done about kinetic studies referred to different materials for various processes.

Among the huge thicket of studies cited, in this section, it will be provided a review of the most interesting for the purposes chosen for the present paper.

The works are here explained and cited, then in following chapters, their proper ideas and methodologies are used to analyze the use of the SFNM perovskite for the chemical splitting of carbon dioxide and water, which represent the singularity of the whole thesis, as forewarned in the subchapter 1.4.

The main works, on which the whole study is based, are represented by the ones published by the research group associated to the main mentor Massimo Santarelli and their collaborators.[6] [7]

The cited projects are grounded on similar processes but implemented with different materials compared to this analysis. The biggest difference is represented by the use of the Ceria instead of the SFNM perovskite; this choice let the temperature drop down, especially during the material oxidation, which in the previous study was stated at 700°C, while, in the present one is fixed at 500°C.

The job done by A.E. Farooqui et al. is made following a typical schematic for a kinetic analysis. The oxidized/reduced material is posed under the influence of the oxidizing/reducing flow with proper mixture concentration and the variation of the gas composition after reaction with the material is measured.

The aim is realized using a simple microreactor, composed by an Alumina pipe, where a sample of the tested material (Ceria) is placed in powder form – blocked by analytic quartz wool – a gas feeding system to provide the desired gas mixture to the sample, and by an electric furnace used to provide heat for reactions, keeping the process isothermal. A gas analyzer at the outlet provides the measure of the evolution of the gas mixture composition during the reaction. The variation of gas composition during time is related to a kinetic model of the reaction.

The kinetic study is implemented in different steps, at first, the model typology for the reaction is defined, to describe the kinetic parameter, the rate constant, described in the following chapters of the present (especially the third one).

The results of the work show that the CO_2 splitting is increased by the thermal level rising, in a similar way, the same behaviour is acquired enlarging the carbon dioxide concentration (doubling it, the CO production quadruples).

In the proper evaluation for the kinetic information, a mathematical technique is carried out. The choice of the best model, among the varying that which can be applied, is determined using the F-test.

From the fitting of the empirical curve, the one referred to the α parameter, respect the theoretical one (calculated though the model), proper values, of the activation energy and frequency factor, are determined.

In the *Fig.4* it is shown the correlation between the α term, derived by the mass calculation, normalized and the models chosen for the comparison. This step will be explained more in details in the chapter 3 of this dissertation.

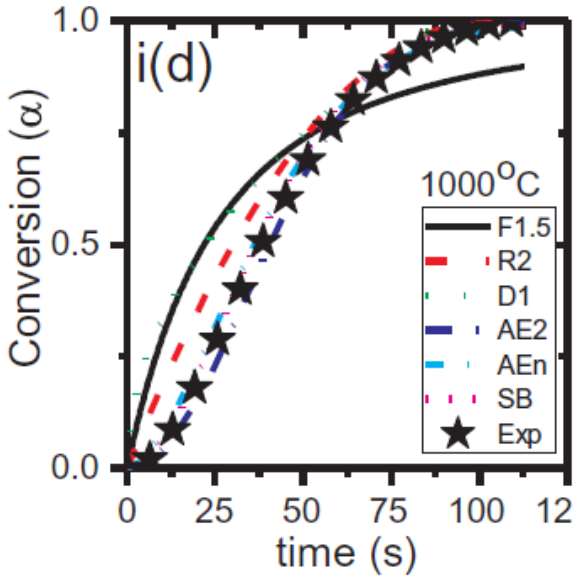

Figure 4 - Comparison of α vs. time between the experimental data and models with a concentration of 20% of CO2 at 1000°C using Ceria

Here, a consideration is necessary. The authors were able to compare the results, of both parameters cited, respect the huge amount of literature existing for the theme. This difference, respect the actual work described in the following chapters, is substantial. The real innovation of the material analyzed (the SFNM perovskite) gives to the work an exciting point of view for the topic chosen, reversely, it will represent the main problem, whit which it makes difficult dealing, owning a significant lack of contrasting, the results will be able to be validate following empirical analysis (it will be done in the final chapter of the work, the number 5).

Following the path suggested in the previous paragraph, some interesting considerations could arise from the work[8] elaborated by H. Ebrahimi and M. Rahmani.

In the cited analysis, in a reverse way, respect the A.E. Farooqui et al. case, the feature of the study, which links to the current study is related to the use of a perovskite ($La_xSr_{1-x}FeO_3$, $LSF731$) in the chemical looping; although the material is different, in terms of metal doping, results can be taken as blurred pathway.

The researchers bumped into the same problems, due to the lack of information for the kinetic evaluation of the material, complained few rows above. For this aspect, a dynamic evaluation of the syngas production has been carried out.

The kinetic procedure remains the same: the α term is calculated through a Thermo Gravimetric Analysis, TGA (method explained more in details in chapter 2 of the present thesis), and it is used in a correlation together with the constant rate for the reaction rate calculation (this second step is the proper kinetic one, elucidated in the chapter 3 of this paper).

The authors conclude the work evidencing the best models to fit the solution, underlying that the couple of methods, with the highest statistical information (used to quantifying the validity of the method for that proper implementation), belonged to the same group of reaction evolution, the reaction-order ones.

In a proper outlook related more strictly to the material analyzed in this work, there are few papers which describe their own approach with the SFNM. Although the applications used are different, for several point of view, information for the material are always useful in order to achieve a more complete panorama.

To achieve the aim purposed, in this section, some works[9] will be cited.

The paper prepared by S. Hu et al. analyzed the SFNM perovskites in a detailed point of view, with the aim, related to their characteristics, in the use as material for an electrode in a SOEC (Solid Oxide Electrolyzer Cell).

Among the group of perovskites researched, there is also the one used here, the $Sr_2FeNi_{0,4}Mo_{0,6}O_{6-\delta}$.

The application in the context of the electrochemical field is very usual. This commonality is explained by the specific features of the material in object. Betwixt them, the main ones mentioned are: the redox steadiness and the opposition to coke generation.

More interesting are the negative issues related to the oxidation of the material, under the effect of the oxidizing CO_2.

The cited paper underlying strongly the consequence of the Nickel doping amount stayed in the perovskite. The metal residence, in the B-site of the oxidized material, let the stability, of the reaction, dropping down. In spite of the huge incrementation of the activity, once faced with the carbon dioxide, the perovskite oxidation gives birth to some carbonates, at the expense of the CO generation.

In fact, the main desirable reaction (to simplify) would have to be to one cited in Eq 2, derived by the general explained in this same section, the eq. 1:

$$Sr_2FeNi_{0,4}Mo_{0,6}O_{6-\delta} + CO_2 \rightarrow Sr_2FeNi_{0,4}Mo_{0,6}O_{7-\delta} + CO + Heat$$

Equation 2 - SFNM oxidation by CO_2

But, for the reason announced just now, it happens that, in some cases, the occurring reaction is:

$$Sr_2FeNi_{0,4}Mo_{0,6}O_{6-\delta} + CO_2 \rightarrow Sr_{2-X}FeNi_{0,4}Mo_{0,6}O_{7-\delta-Y-3X} + X\,SrCO_3 + Y\,CO + Heat$$

Equation 3 - Strontium Carbonate formation from SFNM reaction with CO_2

In the case of the reduction, using a blend containing H_2 the reaction produces $SrMoO_4 + H_2O$.
While, the simplified theoretical reducing reaction it would be:

$$Sr_2FeNi_{0,4}Mo_{0,6}O_{6-\delta} + H_2 \rightarrow Sr_2FeNi_{0,4}Mo_{0,6}O_{5-\delta} + H_2O$$

Equation 4 - SFNM reduction by H_2

The formation of these two compounds depends on the feeble Nickel-Oxygen chemical bond. This aspect, seems that it could be prevalent respect the benefit generated by the Iron-Nickel matching with CO_2 during the process.
The formation of these aggregates implies some issue, which have to be highlighted.
In fact, although the field of application, of the S. Hu et al. work, is different, respect the one analyzed in this master thesis, the damage aroused by the $SrCO_3$ and $SrMoO_4$ formation could be strongly affecting also in the chemical looping (without electrochemical excitation, the environment in which the S-Hu et al. paper deals with) exploitation.
The aggregations, formed by the Strontium, indeed, elicited the strongly known carbon deposition, which reduces the charge transfer and the oxygen diffusion on the SFNM outer layer.
The charge transfer is perfectly inserted in the theme treated in the work. This phenomenon, indeed, is a kinetic process related to the chemical reaction. To clarify, the event occurs mainly in an electrochemical environment, at the electrodes.
In an electrochemical cell two different half reactions take place, each with the proper own given kinetic; which is strictly related to the reaction rate. In this context, the parameter which evaluates the speed of the electrochemical reaction is function not only of the temperature, but rather also of the potential gradient in the electrodes.
Another relevant annotation made by researchers is referred to the surrounding conditions applied on the perovskite oxidation. The suppling oxidizing gas, indeed, is composed, obviously by pure carbon dioxide, at the beginning; later, the gas is necessarily contaminated by the carbon oxide produced. This decreasing of CO_2 increases significantly the $SrCO_3$ and $SrMoO_4$ generation.
This influence with the process evolution could implicate a starting peak of CO production with a significative shrinking of the carbon monoxide creation during the time evolution.

The phenomenon discussed occurs in the electrochemical environment, as said, but the case studied for the interest, of this investigation, is referred only for a SFNM oxidation promoted by the carbon dioxide, without a voltage implementation and heat providing neither.
In any case, the debated aspect, related to this sort of carbon deposition, could occur also in the proper status, therefore, during the experimental phase, it is fundamental keeping in mind the issue.

2. Thermogravimetric analysis

The analysis began following data and experimental procedures provided by UniUd, measures using the Thermogravimetric Analysis (TGA) system (model NETZSCH STA 2500 STA2500A-0275-N) are acquired.
In first analysis, a reduction/oxidation tests have been implemented, cycling TPR and TPO, using, as oxidant, air and, then, diluted CO_2.
Through the TGA, is observed if the material is reducing, losing weight or oxidizing, if it gains weight.
So, to characterize the material, a Temperature-Programmed Reduction (TPR) and a Temperature-Programmed Oxidation (TPO) has been applied.
The reduction ramps are made with a reducing blend, made with Hydrogen in a 1% concentration and in a temperature range: from 0 to 900 °C (this upper boundary is chosen to avoid change in molecular structure of the material).
With this method, it is possible to see at which condition the reduction (TPR) or oxidation (TPO) occurs.
This method has been made in a cyclic way.

In the exit of the TGA, using a mass spectrometer, the composition of products is known, seeing how much hydrogen there is, measuring the partial pressure; the lack of it implicates the reaction with the sample. In case of oxidation, Carbon monoxide (CO) is produced, although this parameter can be misunderstood with the Carbon dioxide (CO_2) by the gas analyzer, because of the similarity of the compounds. Another important consideration has to be made in relation to the water production, after an hydrogen reduction, it could condensate on pipes, since the amount of the production is really poor; this value is not reliable.

In the machine, near 10 mg of perovskite is inserted. In the bottom part of it, Argon, as inert gas, is injected. Then, the reducing/oxidizing blend flows around the sample.
The green line, in graphs reported in Section 2, shows the relative mass measured in the TGA. Before starting the experiment, an heating of the tester is executed, to eliminate oxidizing species.
The mass is constant until the reduction starts (in a 1% Hydrogen blend, diluted in Nitrogen); it begins losing mass. The reduction is carried out until the environment conditions are reached; here starts the CO_2 injection at 500°C, to oxidize the bulk, carried out until 900°C; where the cycle restarts.

The results of the TGA test has been provided to the Università degli studi di Udine (UniUd), which, through X-Ray Diffraction (XRD) and Scanning Electron Microscope (SEM) analysis, can observe the amount of carbon deposition, to evaluate the possibility for an injection of air, to burn it.

The TGA is a method used to characterized a material. This method, as described, consists in the practice of a sensitive, high precision balance, surrounded by a technical furnace, which can reach extremely elevated temperatures[10].

The instrument detects the mass variation of a sample – measured as difference with respect to a reference weight – during the thermal process. Thanks to the huge sensitivity, also the littlest mass variation can be measured, in the order of micrograms.
The application has several degrees of interest in the material characterizations[11] [12] [13], especially if it is paired up with other procedures[14], as mass spectrometry.
The main advantages in the use of the TGA, as first steps for the material discovering, is its relatively low cost (the main one, quite big, is represented by the instrument itself) and its speed and accuracy of the results[15].
To avoid gradient in the researching material, a pulverized sample is suggested[16].
Especially in the use carried out in this study, where solid/gas chemical reactions occur, at isothermal conditions. In fact, one of the application in which the method is implemented is exactly the reduction/oxidation action of a material[17], in addition to its stability behaviour[18].

2.1. Experimental setup description

The device used is a thermogravimetric balance, which can measure mass variation in function of time; controlling the thermal environment and the chemical atmosphere.
The system is composed, mainly, by a furnace, which can work in thermal conditions up to 1600°C and a differential balance system, composed by two arms, connected to the furnace and the crucible (where the sample is laid), this component has a resolution around 0.03 µg. The differential mass value is obtained through the compensation system, composed by two magnetic coils, which through optical signals, properly converted electrically, give the information of the measure.

Figure 5: TGA NETZSCH STA 2500 STA2500A-0275-N[19]

2.2. Experiment

Explaining more in details, what said in the previous chapter 1:

The “zero” step is carried out, trying the crucible, made in Platinum, and verifying that no mass-variation occurs when the crucible is subjected to a test cycle with the same temperature and gases of the real test condition. This obvious consideration is directly represented by the flat green line, and it is explained by the lack of the sample inside the crucible; so, no variation in mass occurs. The procedure is implemented blowing Argon (Ar) on crucible for 5 minutes, increasing temperature until 773.15 K, using an equally weighted in volume Air/Ar mixture.

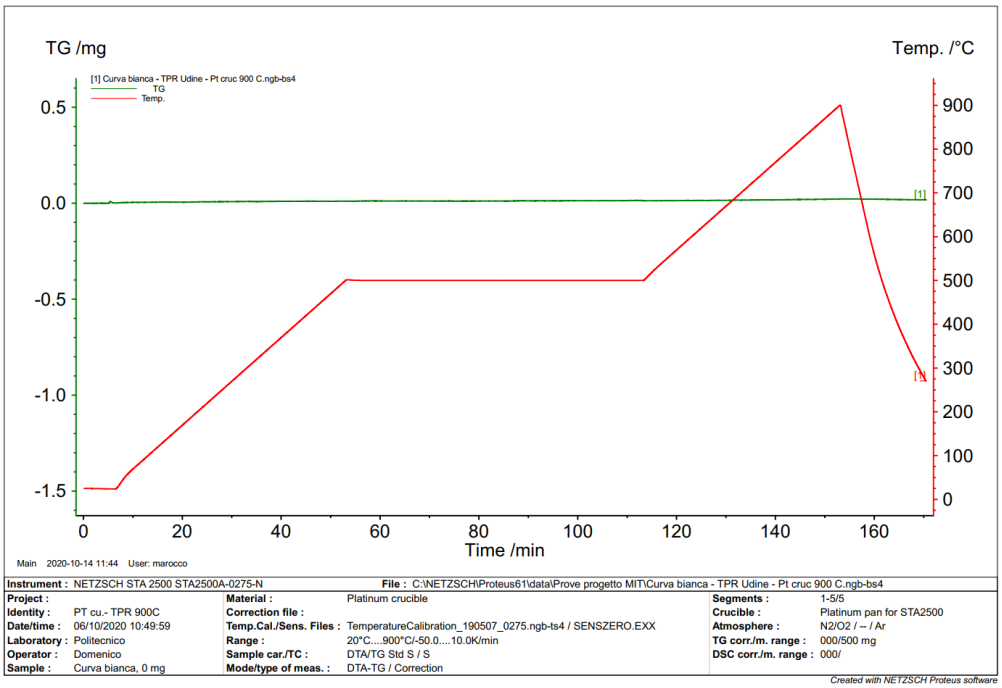

Figure 6- TGA White curve.

After the blank test, the sample (exactly, 16.864 mg) is put in the crucible and then, as represented in *Fig.7*, a pre-treatment in air from ambient temperature to 900°C is realized, to get the sample ready for the reduction/oxidation cycle, eliminating eventually species present on the sample, residual of the synthesis phase. This step is always accomplished, before each test on each new sample.

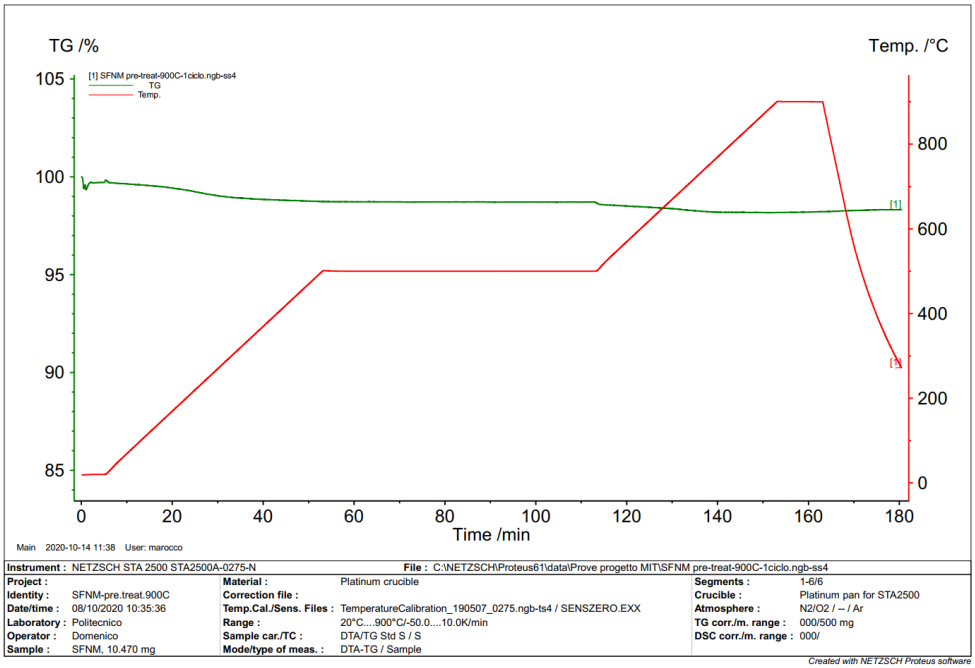

Figure 7 - Air pre-treatment.

The slight drop of mass variation is an evidence for the presence of some contaminants (mainly volatile compounds) on the perovskite.

2.3. Results

2.3.1. Results for air oxidation

A series of cycles of TPR and TPO is realized to test the reduction with hydrogen and the oxidation with air.

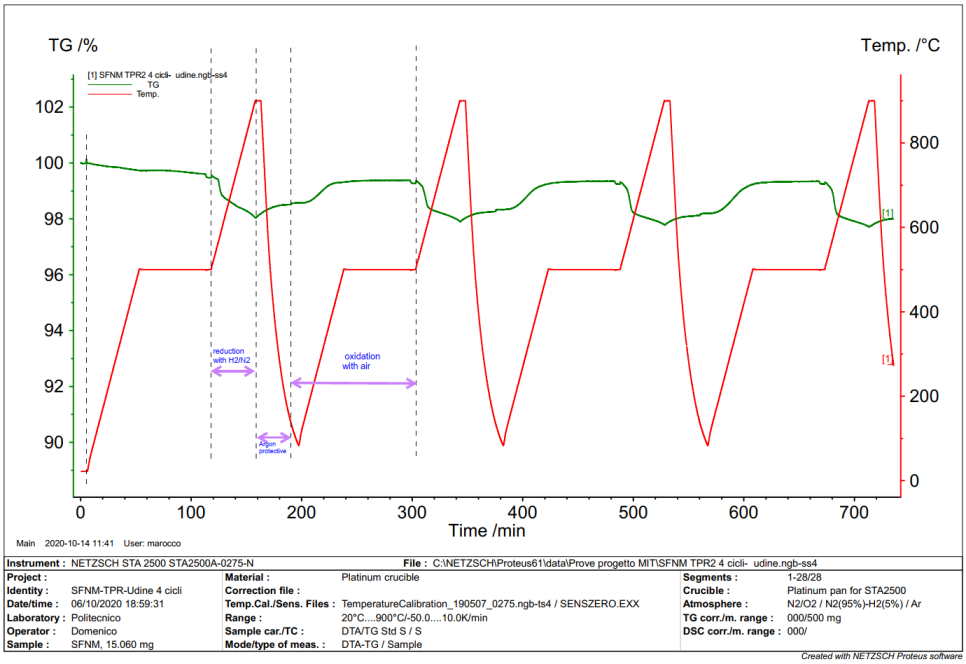

Figure 8 - TRP and TPO 4 cycles with oxidation in air.

The TPR is realized using 1% H_2 in Nitrogen, reducing the sample from 500°C to 900°C. In this step, the mass decreases drastically, as represented in *Fig. 8*. After cooling the sample to ambient temperature, the TPO is carried in a 20% of O_2 (i.e., air) and also this phase is very swiftly, in fact, reached the maximum oxidation temperature (500 °C), the phenomenon stops, while conditions are still provided, the green line stay flat in time. Following, in *Tab.1* is resumed the procedure applied:

Procedure

Number of step	Thermal range	Time	Injected gas
1	298.15 K to 773.15 K	47.5 min	(Air + Ar) 80 ml/min
2	773.15 K	60 min	(Air + Ar) 80 ml/min
3	773.15 K	5 min	Ar 80 ml/min
4	773.15 K to 1173.15 K	40 min	(H_2 (1%)/N_2+ Ar) 80 ml/min
5	1173.15 K	5 min	(H_2 (1%)/N_2+ Ar) 80 ml/min
6	1173.15 K to 298.15	18 min	Ar 80 ml/min
7	298.15 K to 773.15 K	47.5 min	(Air + Ar) 80 ml/min

Table 1 - Air oxidation procedure during TGA testing.

This values are similar to results supplied by Università di Udine.

An interesting observation, was remarked about the reacted hydrogen during all reductions, which was growing for every cycle. This aspect can show a sort of an activation of the material, varying its features during the chemical process. Also this aspect is confirmed by the cited university.

In graphs collected in the *Fig. 9*, the indicated value is representing for the integral of the trend.

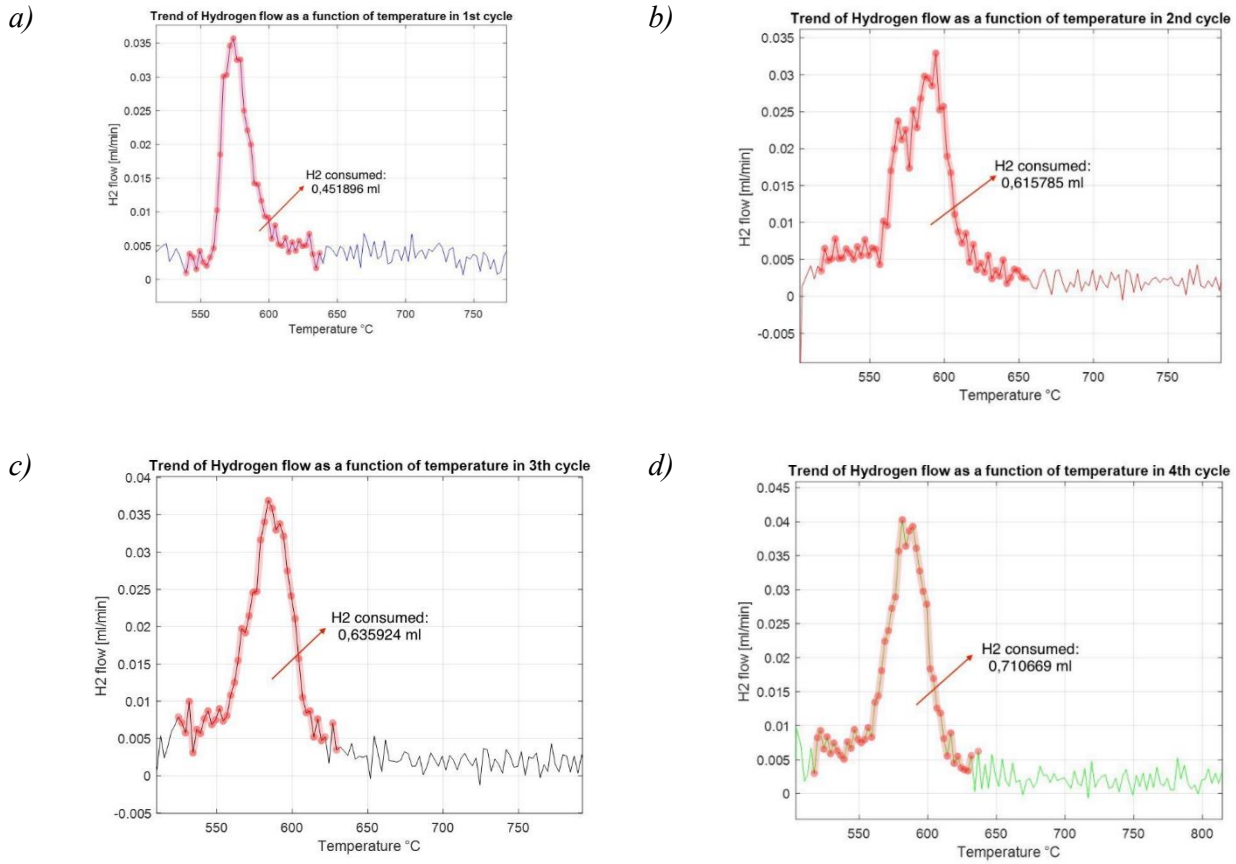

Figure 9 - a) H2 reacted as function of temperature in the 1st cycle; b) H2 reacted in the 2nd cycle; c) H2 reacted in the 3rd cycle; d) H2 reacted in the 4th cycle

2.3.2. Results for Carbon Dioxide oxidation

This section is the real core of analysis for the second chapter, because of the interest for this application. Experiments are lead oxidizing with a blend composed by CO_2 and Ar, keeping the reduction as in the sub-chapter 2.3.1.

The procedure for this subdivision is the same as the air oxidation hereby described is represented in the *Tab. 2*, to make easier the comprehension:

Starting from ambient temperature to 900°C, at heating rate 10 K/minute in a dilution of H_2 (1%)/N_2 40 ml/minute + Ar 40 ml/minute. Then isothermal conditions are kept for 30 minutes at 900°C still in H2/N2 flow + protective gas, reaching the complete reduction. The final 5 minutes at 900°C are used to change the flow to only argon protective 80 ml/minute. A cool down until 500°C at 10 K/min with argon protective 80 ml/minute is necessary, at 500°C, a 5 minutes step, with Argon alone 80 ml/minute, is necessary to complete the pre-cleaning of the system and prepare it for the oxidation. The isothermal oxidation is acquired at 500°C for 90 minutes, a 20% of CO_2 oxidant gas flow is injected. At the end, 5 minutes, still at 500°C, replacing CO_2 with only Argon flow, are carried out. The cycle can restart from the first point with the difference for the initial temperature, which is 500°C instead of 25°C. The whole process is repeated for 4 times, as before.

Procedure

Number of step	Thermal range	Time	Injected gas
0	298.15 K to 1173.15 K	87.5 min	(H_2 (1%)/N_2+ Ar) 40 ml/min
1	1173.15 K	30 min	(H_2 (1%)/N_2+ Ar) 40 ml/min
2	1173.15 K	5 min	Ar 80 ml/min
3	1173.15 K to 773.15 K	40 min	Ar 80 ml/min
4	773.15 K	5 min	Ar 80 ml/min
5	773.15 K	90 min	(CO_2 (20%)/N_2+ Ar) 40 ml/min
6	773.15 K	5 min	Ar 80 ml/min
7	773.15 K to 1173.15 K	40 min	(H_2 (1%)/N_2+ Ar) 40 ml/min

Table 2 - CO_2 oxidation procedure during TGA testing.

The final provided results are:

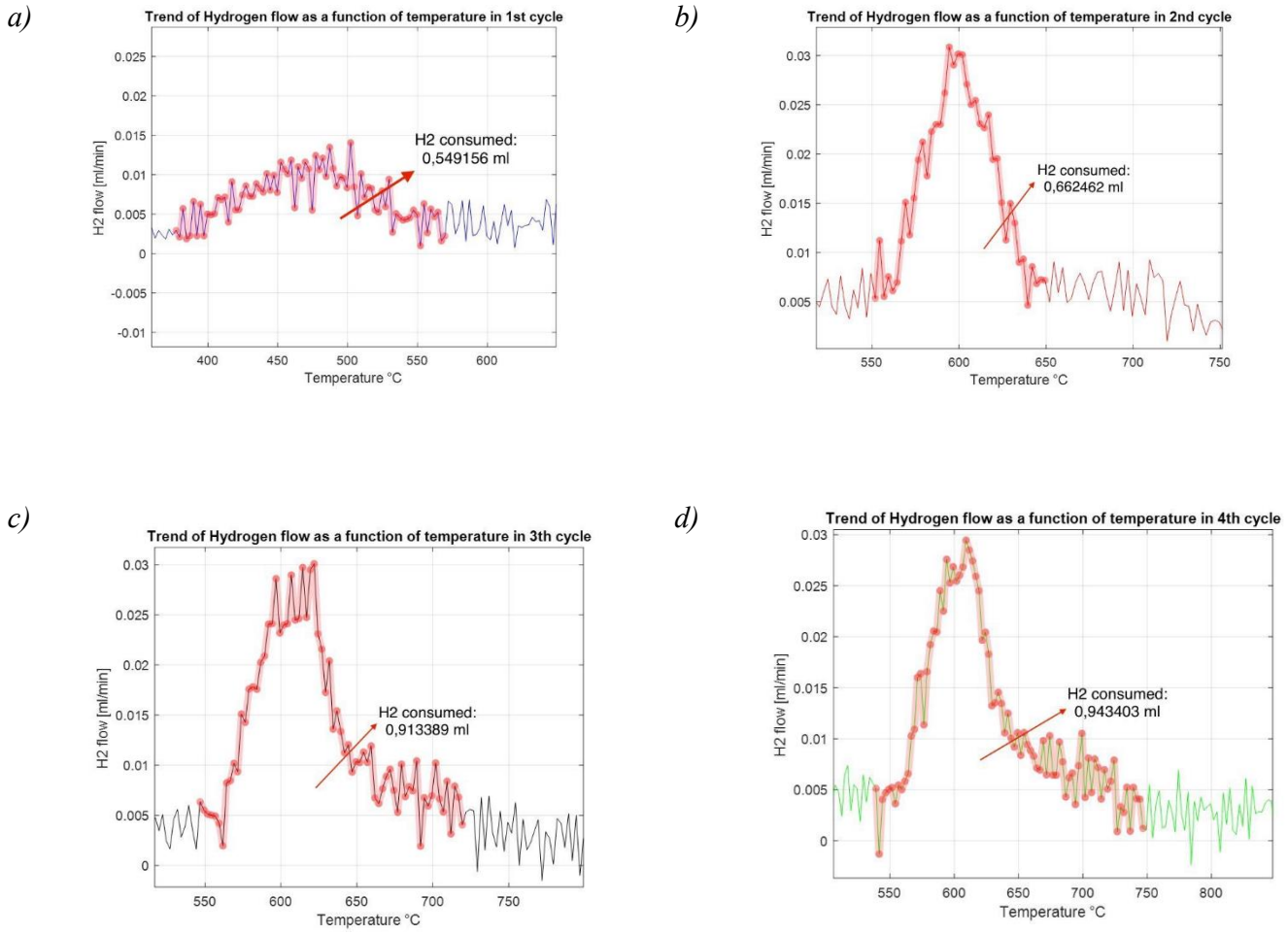

Figure 10- a) H2 reacted as function of temperature in the 1st cycle; b) H2 reacted in the 2nd cycle; c) H2 reacted in the 3rd cycle; d) H2 reacted in the 4th cycle

The material shows, as the oxygen case, that the produced hydrogen keeping growing in each reduction step, moreover, the cycling of the perovskite is confirmed.

This SFNM can be oxidized by the carbon dioxide, as well as oxygen, in particular it is interesting this availability in this thermal range.

To verify the durability of the material in a stricter cycling process, a new experiment is carried out and cycles are increased until 10 repetition, using, as oxidant, a mixture of CO_2 (20 %) and Argon.

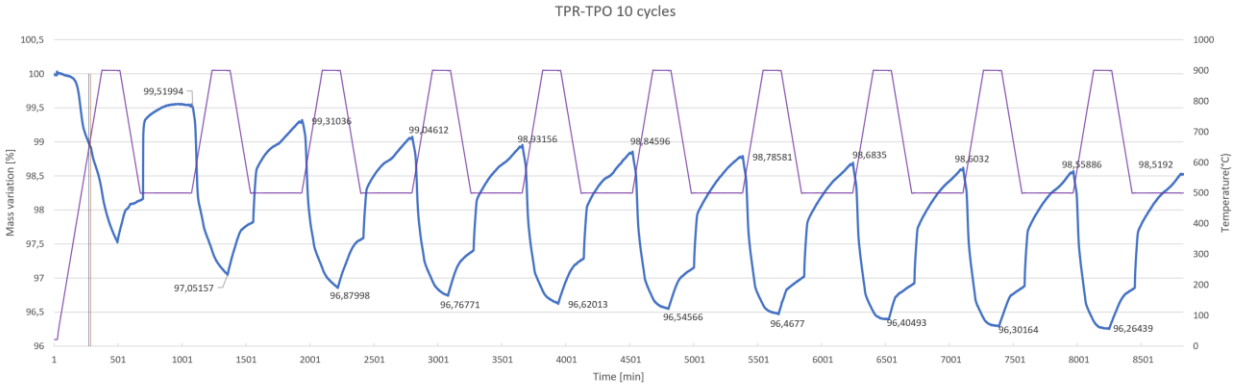

Figure 11 - TRP and TPO 10 cycles with carbon dioxide.

The samples used in the experiments have been conserved and sent to Università di Udine to investigate if some atomic structural deviation has occurred.

The tests, implemented by the Friulian department of chemistry, Physics and environment, are executed using the X-ray scattering technique. This method, simplifying, works using a ray emitted by the machine, which was captured by a receiver. In according to the tilt angle at which the radiation was captured, it can discriminate which compound there is in the sample.

The results obtained, represented in *Fig.12*, give some interesting considerations.

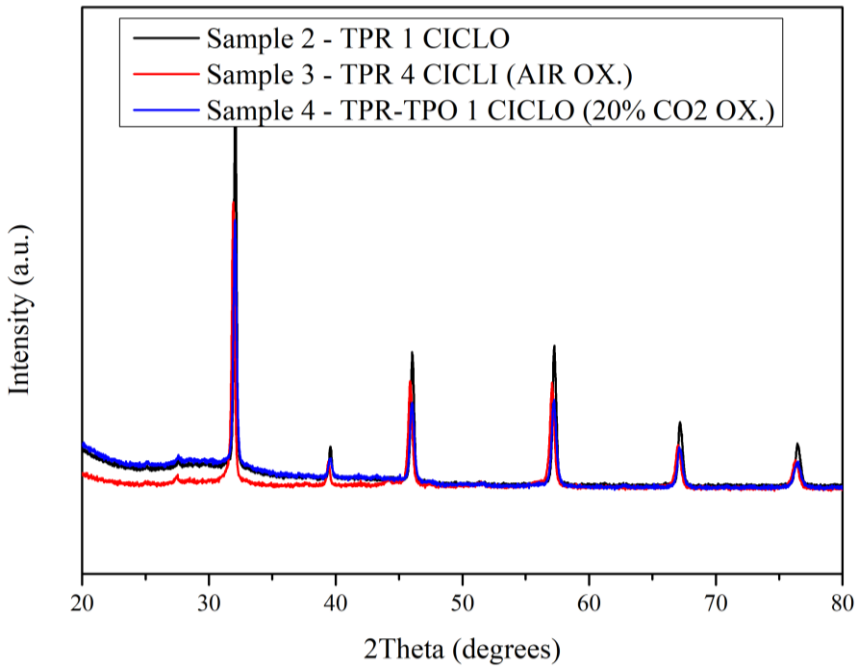

Figure 12 - XRD analysis for samples 2, 3 and 4 provided by the department of Chemistry, Physics and Environment, Università di Udine.

The researchers have noticed that the sample number 3, got oxidizing in air the SFNM, has the best structure; that is why near 44.5° has been detected a Ni-Fe alloy, which operates as catalyst for the reaction. This phenomenon, under the effect of the carbon dioxide doesn't occur.

Confirming the occurrence predicted in the introduction, it has been encountered $SrCO_3$ and $SrMoO_4$, which, diversely respect the Ni-Fe alloy, act as electrochemical insulator. The strontium carbonate and the strontium molybdate occur in all the tests, in any oxidizing conditions.

The positive effect measured, in other hand, is that, treating the sample at 800°C, oxidizing with air for one hour, these agglomerates were re-absorbed.

Sample	*Procedure*
2	1 cycle
3	4 cycle in Air oxidation
4	1 cycle in CO_2 oxidation
5	10 cycles
6	6 cycles + long oxidation
7	6 cycles + long oxidation and reduction

Table 3 - Samples furnished at the end of the TGA step.

In *Fig. 13* are represented the same analysis for the remaining samples, obtaining in the final TGA step, oxidizing for 10 cycles the taster 5, for 6 the sixth and reducing in the final time step the sample 7.

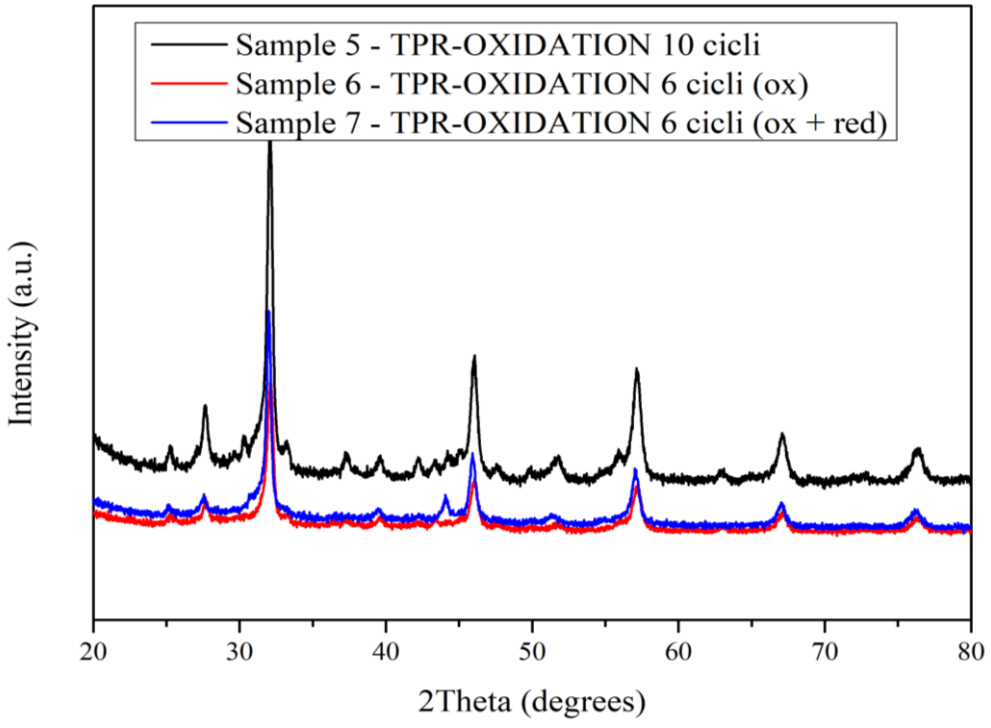

Figure 13 - XRD analysis for samples 5, 6 and 7 provided by the department of Chemistry, Physics and Environment, Università di Udine.

As resumed in *Tab. 3*, the sample 6 and 7 are submitted to a different-in-time procedure.
The number 6 dealt with a 6 hours oxidation (near 6 times more than the others)
The sample number 7, has been obtained adding, after the 6 hours oxidation, a 6 hours reduction, carried out at 900°C; this change in the procedure is applied to understand how much the sample could be totally reduced.
The structure of the material shows that the two negative compounds, the $SrCO_3$ and $SrMoO_4$, are participating, together with the Fe-Ni alloy, which is significatively there.
So, to summarize, the researchers of the Università di Udine have confirmed that the Ruddlesden-Popper phase, the typical perovskite structure, was born. In addition, it seems that the Fe-Ni alloy formation occurs, but, to confirm it, it is necessary a Field Emission Scanning Electron Microscopy (FESEM) analysis, using alloy nanoparticles exsolution of comparable size; although, through the Energy dispersive X-ray (EDX) spectroscopy, there is a first validation of the alloy generation; due to the long reduction.
As dramatic event the strontium carbonate and the strontium molybdate are found in all the samples. Some suggesting testing, to understand the impact of them on the CO production, could be an exposition of the material at a hydrogen reduction at a lower temperature, to highlight the real weight of the exsolution. Then, it could be applied an oxidation at 800°C. Finally, it could be significative an oxidation at 850°C, to dissolve the negative compounds generated.
Some stability tests are necessary, increasing the temperature, the $SrCO_3$ and $SrMoO_4$ could be absorbed, this answer could be given by the stabilization of the growing mass deposition during the experiment.
In any case, an air or N_2 pre-treatment at 850°C for one hour is suggested.

3. Kinetic model

A kinetic evaluation is always necessary to evaluate the proper feasibility of the reaction implementation, in the field purposed by the aim.

More specifically, the intending analysis is referred to the oxidation phase of the process, since the reduction of H_2 happen in any conditions.

The study has to investigate the potential rate of reaction for the chemical process in the microreactor, estimating efficiencies and performances.

The aim is acquired, performing the fitting of an isothermal oxidation test in TGA at temperature of 773.15 K, measured while the CO_2 concentration was 20% in the mixture of the oxidant.

The choice for the correct kinetic model is done using chemical (fitting reactions models at measured conditions) and statistical (root square mean error) considerations.

A typical methodology, to evaluate the quality of the fitting between empirical results and the model ones, is the Akaike Information Criterion (AIC). This procedure is based on the evaluation of the vanished information through the passage from experimental data and their modelized description. One of the negative effects of the criterion is that it can't notify the suitable fitting of the model.

3.1. Typologies of models

Mainly, kinetic models are subdivided in 4 categories, in according to the prevalent mechanism of evolution of the reaction.

Nucleation models, also renamed Avrami-Erofeev models (AE), are based on the production of nuclei, as the denomination trivially suggests, where the reaction occurs. During an oxidation, the single reactant particle grows until it melts with another particle nearby.

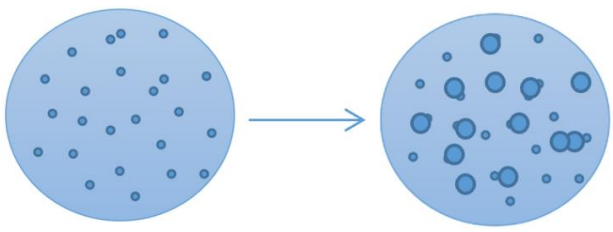

Figure 14 – Nucleation model scheme.

Diffusion models simulates the phenomenon of the reaction considering the evolution occurring in the front of external boundaries; considering the reactant as a sphere, it grows (in case of oxidation) radially.

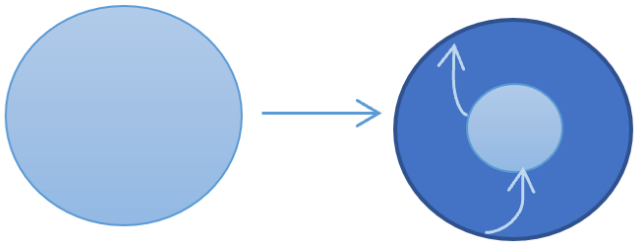

Figure 15 - Diffusion model scheme.

The reaction order models are the ones which simplify the problem with an uniform advancement of the reaction, following a standard approach, for which, using an ideal point of view, the chemical response is the same in each part of the reactant place.

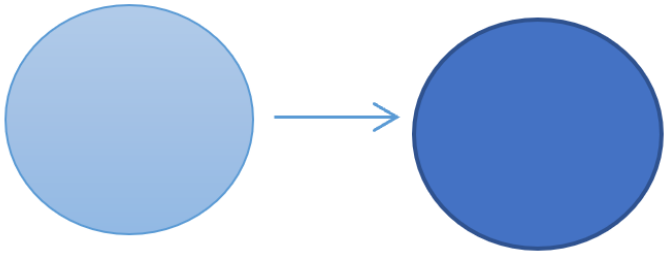

Figure 16 - Reaction order model scheme.

At the end, geometrical contraction models are used to simulate a reaction which occurs on boundaries of the element particle, considering each one with the proper geometry and following the shrinking core mechanism.

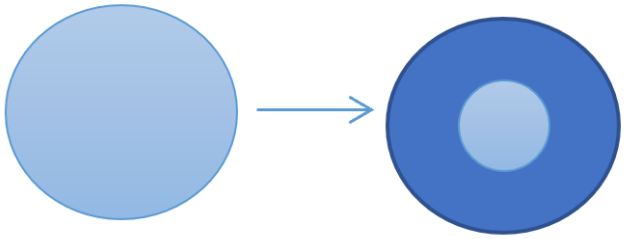

Figure 17 - Geometrical contraction model scheme.

3.2. Kinetic overview

Kinetic conditions in a reaction are fundamental for a quantitative estimation of the time amount necessary to realize a given chemical process. This aspect develops with thermodynamics considerations. In fact, while the first concept gives information about the amount of time to have a reaction, the second aspect describe the effectivity chance, for the reaction, to occur.

A certain reaction reach equilibrium in some conditions, for thermodynamic reasons; although this is true only in an ideal situation, this because the reality has to be face with kinetic thoughts.
The speed of a process is influenced by the nonuniform material properties and the fluid-dynamics of the reactant mixture, the most critical parameter is the speed of it in the reactor; if the residence time is too small (ie. high gas velocity), the compounds might not have time to reach the equilibrium. For this reason, an important parameter, to consider, is the Gas Hourly Space Velocity ($GHSV = \left[\frac{Nm^3/h}{m^3_{reactor}}\right]$)

Kinetics of chemical reactions mainly deal with the rate of a chemical reaction.
For a generic reaction:

$$\nu_{R_1} R_1 + \nu_{R_2} R_2 \longrightarrow \nu_{P_1} P_1 + \nu_{P_2} P_2$$

Equation 5 - Generic Reaction.

Considering $C = \left[\frac{mol}{m^3}\right]$ as the concentration of chemical species, the rate of reaction is given by:

$$r = -\frac{1}{\nu_{R_1}}\frac{dC_{R_1}}{dt} = -\frac{1}{\nu_{R_2}}\frac{dC_{R_2}}{dt} = \frac{1}{\nu_{P_1}}\frac{dC_{P_1}}{dt} = \frac{1}{\nu_{P_2}}\frac{dC_{P_2}}{dt}$$

Equation 6 – Reaction rate for a generic reaction.

This parameter is strongly affected by:

- The type of reaction, so, mainly by the compounds phases.
- The temperature, high temperatures means high vibration speed of particles, increasing the probability to collide, together with the proper rate of reaction.
- The concentration, high concentration means larger number of particles, larger number of particles increases the frequency of collision and therefore the own rate.
- The presence of catalyst in terms of type, quantity and active surface. This component participates to reaction without change itself, it reduces the activation energy, modifying the energy pathway.

From the law of mass action, according the which a direct proportionality between the reaction rate and reactant concentration occurs, can be derived some interesting evidences.
The cited classical approach for reactor design is a basic knowledge for the correlation between the rate of reaction and macroscopic properties, as temperature and concentration.

The rate of reaction, based in according to this principle is expressed by the eq. 4:

$$r = k(T) \prod_i C_i^{\nu_i}$$

Equation 7 - Reaction rate according to the law of mass action.

In the expression, the $k(T)$ term is the constant rate (described in function of the temperature) and represents the most critical value of the problem.
The numerical value is calculated using the Arrhenius equation:

$$k(T) = k_0 \, e^{-\frac{E_a}{R}\left(\frac{1}{T}\right)}$$

Equation 8 - Arrhenius equation.

Where k_0, the frequency factor, comes from a fitting of experimental data and E_a, the activation energy, shows the minimum energy of collisions between particles, letting the reaction to occur, properly, activating the reaction.
In a catalytic reaction, characterized by several elementary chemical steps, each of them has different kinetic properties.
So, the global reaction rate depends on many other mechanisms of the reaction; from the huge amount of them, the slowest step, the one which have the lowest $k(T)$, will determine the overall speed of the general phenomenon. The cited step takes the label of Rate Determining Step (RDS).

3.3. Reaction rate estimation

In the case of analysis, the rate of reaction for CO_2 oxidation can be estimated using the some assumptions, in first analysis, as follow.

The evaluation of the kinetic model has been performed using the general approach described in the papers cited in the introduction. In fact, notwithstanding the fact that the material has several degrees of innovation, the way to discover a model that describes the global kinetic of its reaction with CO_2 can be the same applied in general to all materials.

The role of the α term is essential. It is obtained from the data measured in TGA during the oxidation step.

$$\alpha = \frac{m(t) - m_0}{m_{end} - m_0}$$

Equation 9 - Normalized mass variation.

The expression in eq. 6, with trivial meaning of the terms, shows the differential mass $(m(t) - m_0)$ respect the reference value, obtained by the difference of the mass at the end of the reaction and the initial one, so the reacted mass $(m_{end} - m_0)$. The term α is the conversion of the reaction and ranges between 0 and 1, representing the extent of the evolution of the reaction from the beginning to the time *t*.
The rate of reaction, in other terms respect the eq. 3, will be given by the expression in eq.10:

$$r(T,t) = {d\alpha}/{dt} = k(T)\, f(\alpha)$$

Equation 10 - Reaction rate in differential form.

This expression is easily solved, improving the shallow expression of the rate constant (eq. 8), given by the Arrhenius equation with the conversion function $f(\alpha)$, picked from the chosen model.
In this formula, the k_0, frequency factor (or pre-exponential factor) and the E_a, activation energy values are iterated to find the best fitting between the theoretical solution and the one generated by models.
Paying attention on the oxidation phase of the process, for the over-mentioned reasons, some considerations are interesting, basing on the results provided by a code implementation using MATLAB R2020a.
To eliminate fluctuation due to transitory phenomena or external parameters, it has been chosen focusing the analysis only for the third cycle.
Integrating the expression above, it is obtained the function:

$$g(\alpha) = \int_0^{\alpha'} {d\alpha}/{f(\alpha)} = \int_0^{t'} k(T)\, dt = k(T)\, t.$$

Graphing this linear parameter, the slope shows the reaction rate.
The last integrating function is obtained through theoretical assumptions and procedures; to introduce empirical considerations, it has been compared with reference to functions integrated from the ones, $f(\alpha)$, in the Table 1, interpolated using data from Thermogravimetric analysis, especially temperatures and mass involved.

Table 4 – Models[21]

Number of model	*Model*	$f(\alpha)$	$g(\alpha)$
Power law models			
1		$4\alpha^{3/4}$	$\alpha^{1/4}$
2		$3\alpha^{2/3}$	$\alpha^{1/3}$
3		$2\alpha^{1/2}$	$\alpha^{1/2}$
4		$\frac{2}{3}\alpha^{-1/2}$	$\alpha^{3/2}$
Geometrical Concentration models			
5	Zero order	1	α
6	2D (or R2)	$2(1-\alpha)^{1/2}$	$1-(1-\alpha)^{1/2}$
7	3D (or R3)	$3(1-\alpha)^{2/3}$	$1-(1-\alpha)^{1/3}$
Diffusion models			
8	1D	$\frac{1}{2\alpha}$	α^2
9	2D	$\frac{1}{-ln(1-\alpha)}$	$\alpha+(1-\alpha)\,ln(1-\alpha)$
10	Diffusion- Jander D3	$\frac{\frac{3}{2}(1-\alpha)^{2/3}}{1-(1-\alpha)^{1/3}}$	$\left(1-(1-\alpha)^{\frac{1}{3}}\right)^2$
11	Ginstling -Broushtein D4	$3/2\,\frac{1}{(1-\alpha)^{-1/3}-1}$	$\left(1-\frac{2}{3}\alpha\right)-(1-\alpha)^{2/3}$
Reaction-order models			
12	First order	$(1-\alpha)$	$-ln(1-\alpha)$
13	3/2 order	$(1-\alpha)^{3/2}$	$2\left(\frac{1}{(1-\alpha)^{\frac{1}{2}}}-1\right)$
14	Second order	$(1-\alpha)^2$	$\frac{1}{(1-\alpha)}$
15	Third order	$(1-\alpha)^3$	$\frac{1}{2}\left(\frac{1}{(1-\alpha)^2}-1\right)$
Nucleation models			
16	n=1.5	$\frac{2}{3}(1-\alpha)\left(-ln(1-\alpha)\right)^{1/3}$	$\left(-ln(1-\alpha)\right)^{2/3}$
17	n=2	$2(1-\alpha)\left(-ln(1-\alpha)\right)^{1/2}$	$\left(-ln(1-\alpha)\right)^{1/2}$
18	n=3	$3(1-\alpha)\left(-ln(1-\alpha)\right)^{2/3}$	$\left(-ln(1-\alpha)\right)^{1/3}$
19	n=4	$4(1-\alpha)\left(-ln(1-\alpha)\right)^{3/4}$	$\left(-ln(1-\alpha)\right)^{1/4}$

Applying models in *Tab. 4*, the following results, in *Fig. 18*, are provided:

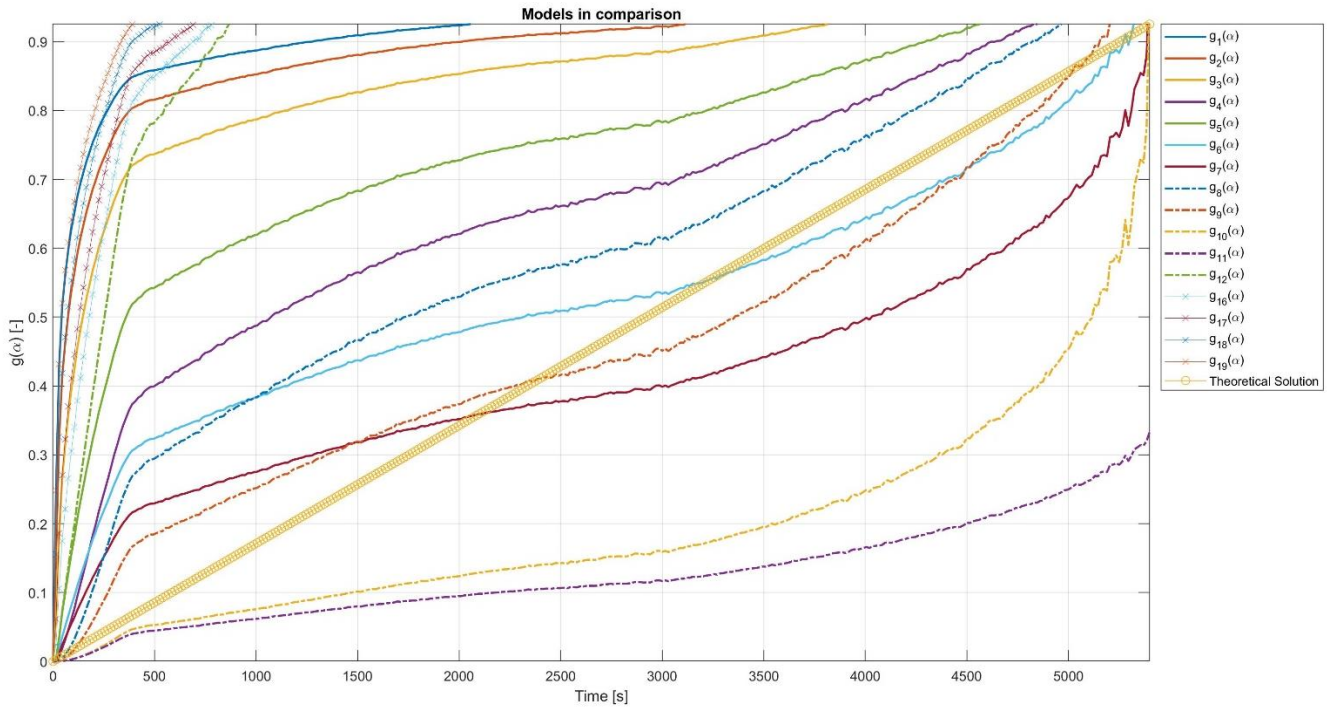

Figure 18 - Models development in time.

It is clear, that only a group of models are fitting the theoretical solution. They are the ones whit the highest coefficient of determination (R^2)[22].

The named coefficient guarantees a well-matching between the model and the theoretical solution, in according to the statistical information.

Estimating the coefficient of determination for the case in analysis (*Fig. 19*), it results clear that some models can be excluded *a priori,* justifying this choice for patterns with a $R^2 < 1$, these are, for several reasons too far from the theoretical solution.

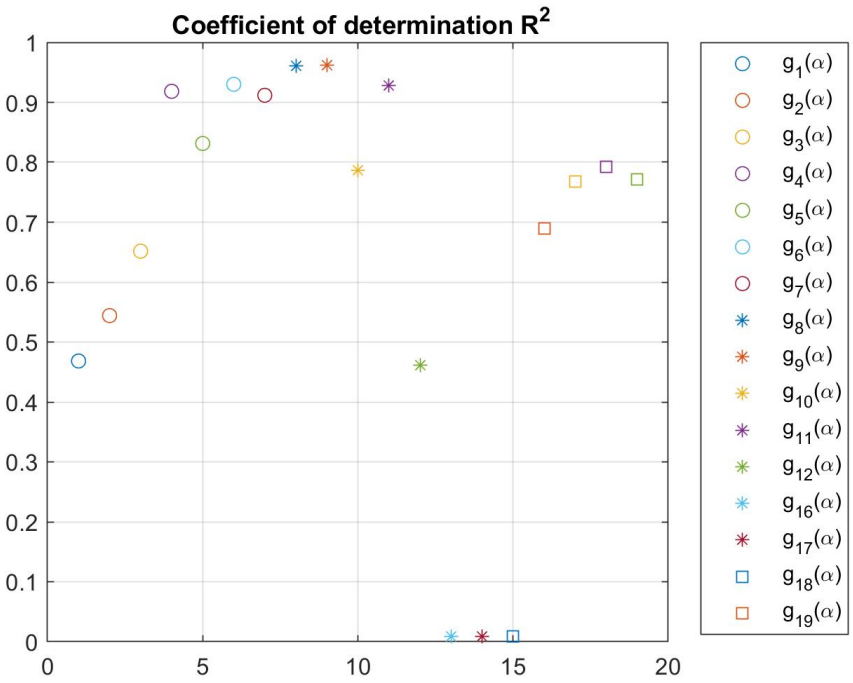

Figure 19 - Coefficient of determination estimation for each model.

Starting from the previous considerations, in first approximation it can be useful focusing the analysis on models: 4, 6, 7, 8, 9 and 11.

An interesting consideration is the fact that half of the six methods extrapolated belong to the diffusion category. This interesting feature of the modeling suggests that the main characteristic of the phenomenon is prevalently dominated by the diffusion modelized process. So, the reaction evolution occurs in the front of external boundaries, the oxidizing reactants, simplified as a sphere, grow radially towards products.

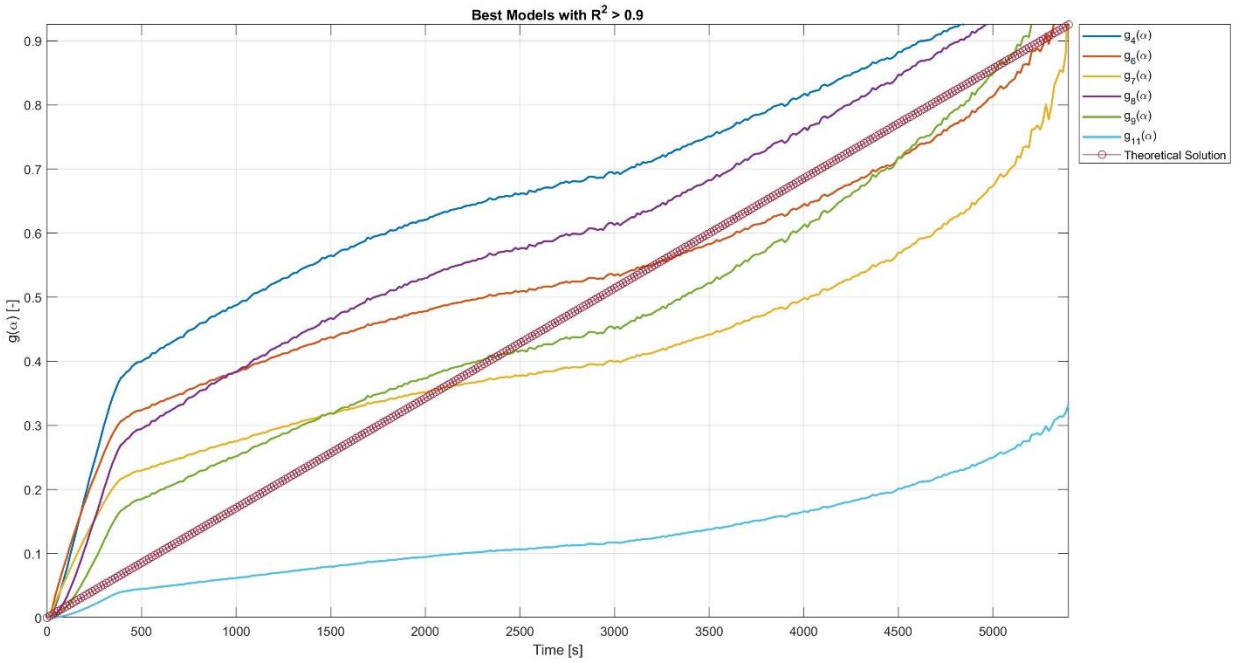

Figure 20 - Best models with highest Coefficient of determination.

An iteration on the frequency factor and on activation energy is carried out, to evaluate the best value, for each model, starting from the value of 75 kJ/mol, for the activation energy and 14 1/s for the frequency factor.

Values obtained are 14.9 1/s and 73,5 kJ/mol, for the frequency factor and the Activation energy, respectively.

The code implemented change iteratively each of the two factors until the squared difference, between the calculated values and experimental ones, minimize the error. The deviation chosen, indeed, is the one described by the mean squared error (MSE). When this error is reasonably low, the iteration stops.

As example, in *Fig. 21*, it is represented graphically the logical method write down in the MATLAB algorithm, to find the best model. The model 7 is drawn in the figure, for brevity it has been chosen only that model, but the same procedure is applied for the ones selected.

This illustration, as reference, is inserted to demonstrate that the worst model (among the six picked up) requires more iteration to reach the convergence of the simulation. The lines (which stand for the theoretical solution), indeed, have different slopes, in according to the value used in that proper run of the algorithm implemented.

The code changes the declination of the line until the error is under the threshold fixed (the tolerance is imposed at 5%).

When the result is obtained, the corresponding value for the frequency factor is memorized.

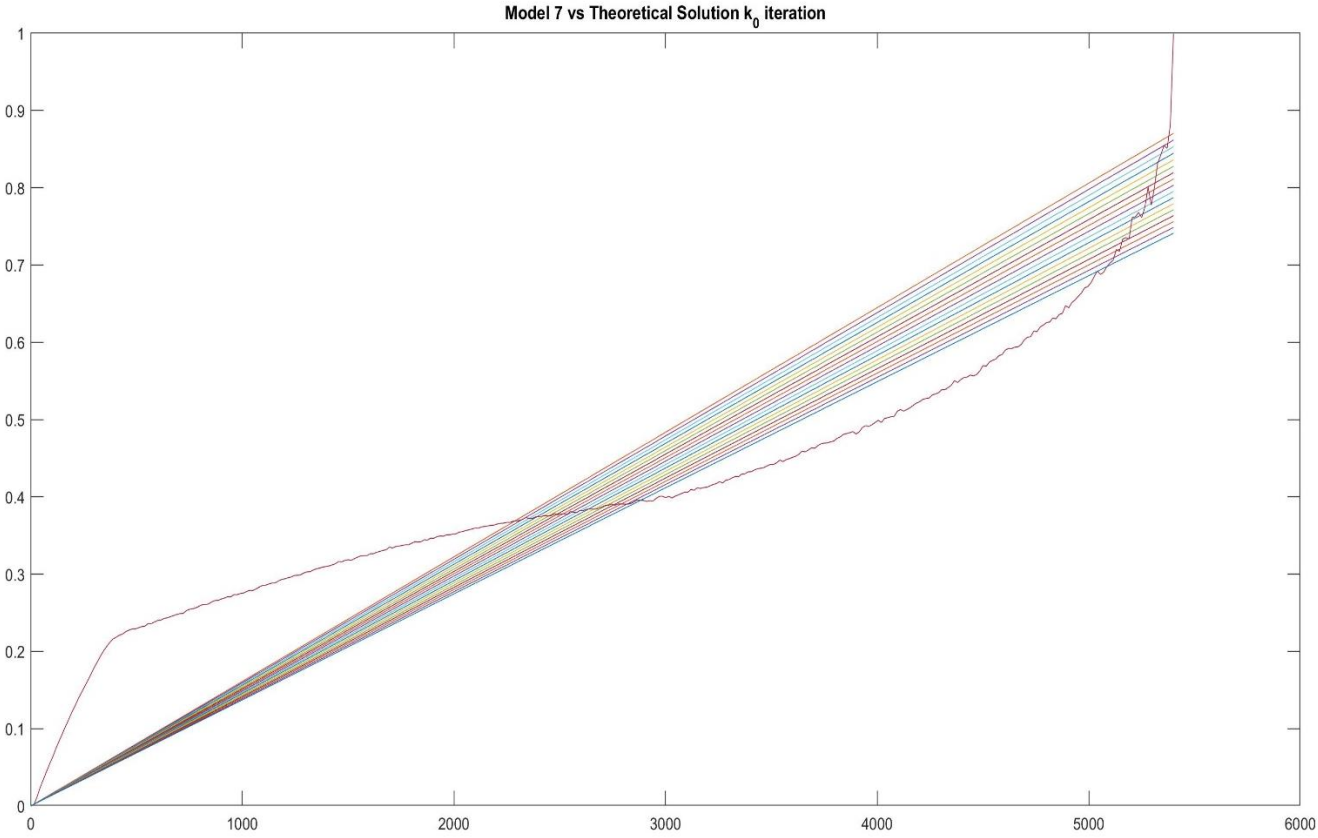

Figure 21 - Iterating implementation, graphical representation as example.

The key parameters, after the iterating implementation, guarantee a coefficient of determination around 0,95 for the model 9, which is the highest obtained.

The same procedure, applied for the best value of frequency factor, is carried out for achievement of the activation energy.

In the case of this last parameter, the iterations are less than the first one, this phenomenon is explained because the range in which can vary the activation energy is several degrees less than the frequency factor one.

Selecting the model 9, because of its best fitting on the theoretical solution, the final stage of the kinetic evaluation can be performed.

The model chosen has a significant adherence to the theoretical solution, and the proper time evolution is reported in *Fig. 22*:

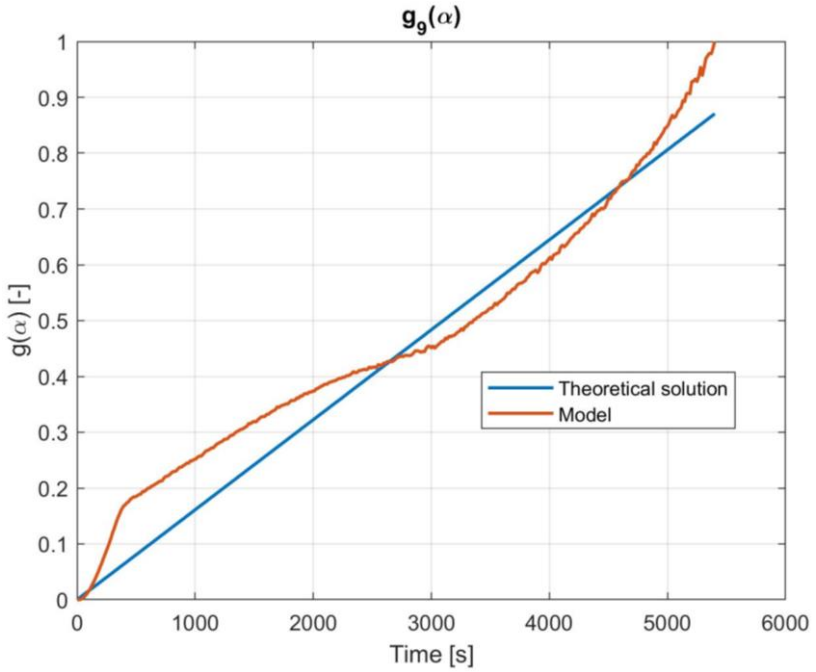

Figure 22 – Best model evolution.

The model is represented by the function in the eq.11, and this is used in the, previously cited, eq. 10, to find the reaction rate value for each time step.

$$f(\alpha) = \frac{1}{-ln(1-\alpha)}$$

Equation 11 - Model 9 function.

The function graphed is drawn in the *Fig. 23*:

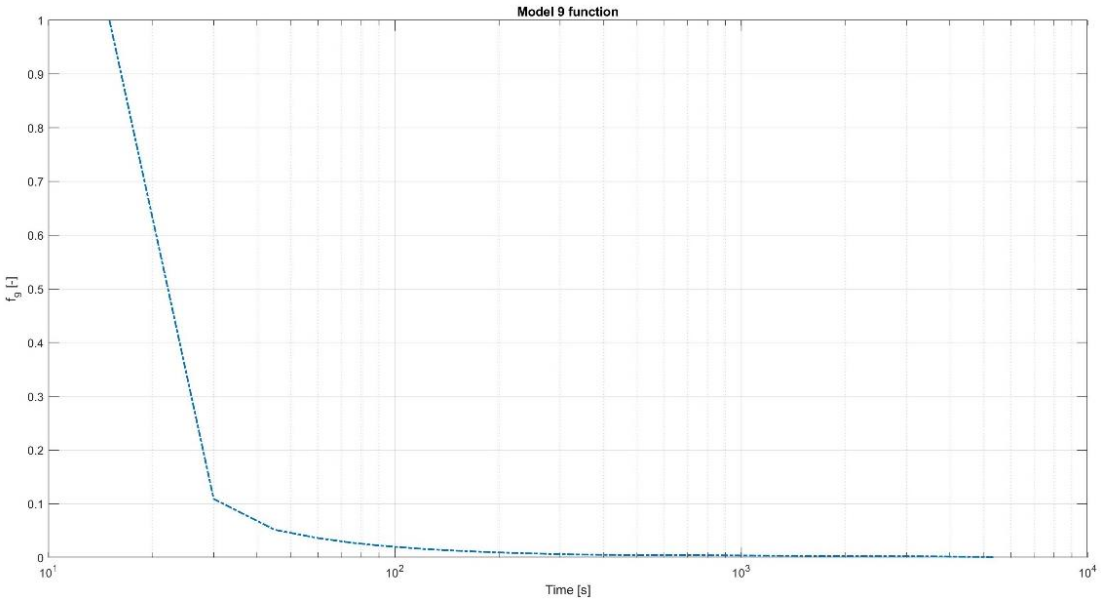

Figure 23 - Describing function model 9.

Obviously, the describing function of the model is the variable which ingrains its tendency to the reaction rate evolution; finally, the real values of the kinetic parameter are impress by the other term of the eq. 10, the constant rate $k(T)$.

To conclude this section, the rate of reaction modelized is represented by the graph in *Fig. 24*:

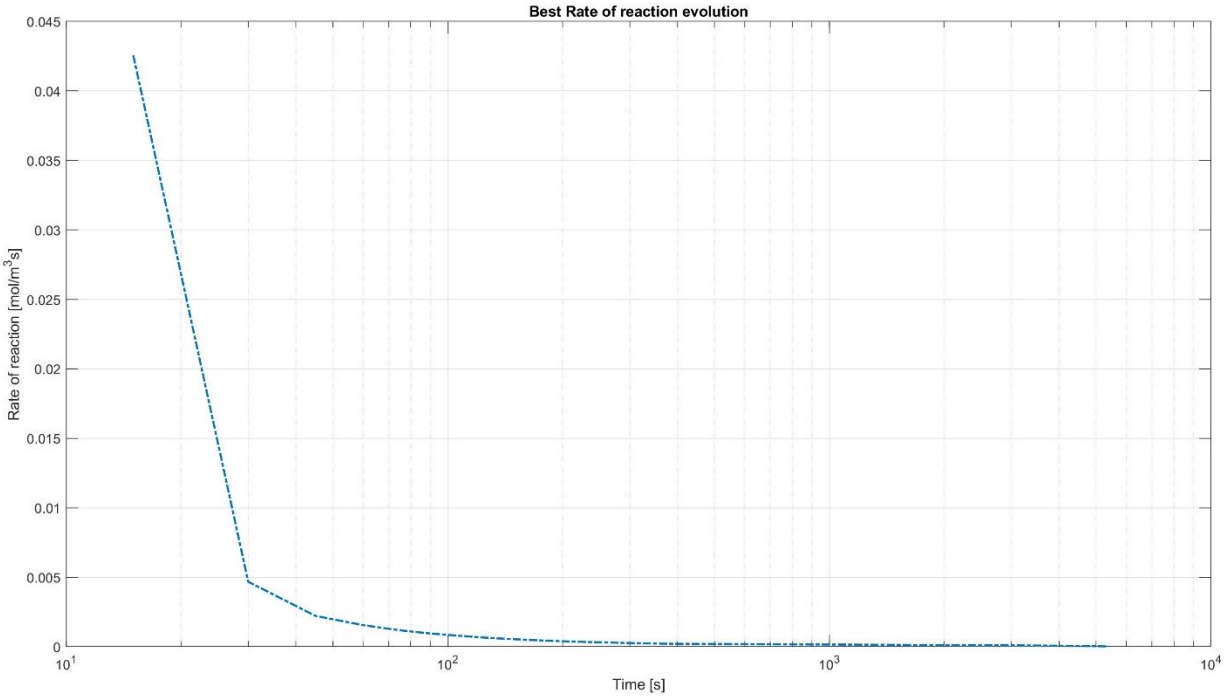

Figure 24 - Rate of reaction evolution (Time in logarithmic scale).

4. Microreactor model

The level of analysis is now switched to the simulation at the level of microreactor of the system studied in the previous section.

The examination is carried out using the solver and Multiphysics software: COMSOL Multiphysics.

To perform the investigation, outputs from fitting analysis, performed in the previous chapter, are used. Values of activation energy and frequency factor, obtained by the fitting, are inserted as input in the chemical setting of the system.

4.1. Geometry, materials and mesh.

The microreactor is modelized as a cylinder, more in detail, as three coaxial cylinders, made in different materials, as reported in *Fig. 25*.

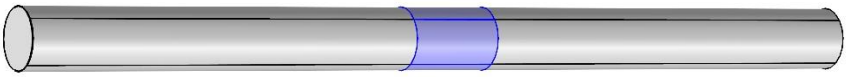

Figure 25 - Component, Microreactor

The outer cylinders are made of an inert material, with good approximation (the only effect is related to a slight variation in the gas distribution) the proper material can be neglected in the modeling definition, and they can be considered only constituted by the mixture of carbon dioxide (20% CO_2 and 80% N_2), which flows inside.

The cylinder in the middle is the core of the component and it is set as a porous medium, made in SFNM perovskite.

About measures, the whole reactor has a length of 300 mm, of which, the SFNM cylinder is length 30 mm.

The diameter of the whole system is fixed at 8 mm.

The mesh built in the simulating software is represented in *Fig. 26*.

a)

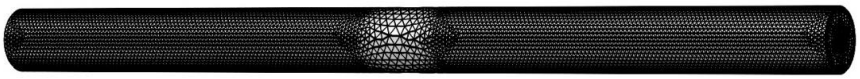

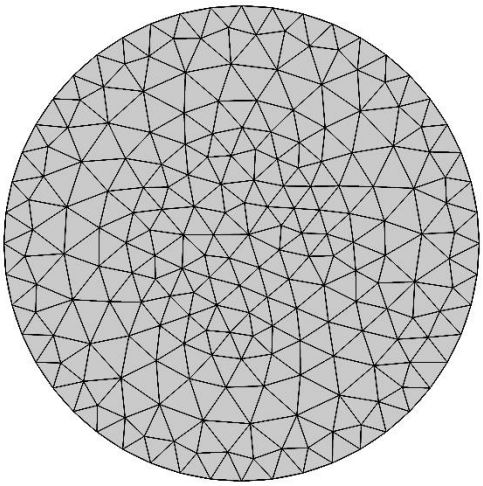

b)

Figure 26 - Mesh used in the component: a) 3D View; b) x-y section view.

The mesh is composed by discrete geometrical elements, these are essential to calculate properties in that specific cells, to understand the estimation of properties variation, along the whole rod.

More specifically, the mesh used is composed by 262930 elements, among these, the majority are Thetraedra (near the 83% of the total elemtents number). The total mesh volume is $9.4 \times 10^{-5}\ m^3$. As quality measure has been chosen the Condition number, this has a value of 0.746, so, being it striclty below the unitary value, the system can be considered as well-conditioned, an optimization, of this parameter, will not be implemented.

4.2. Physics

The Physical phenomenon is simulated using two main Physics: The Transport of Concentrated Species in Porous Media (a subcategory of the Chemical Species Transport), adding Brinkman equations.

Through an additional mathematical environment, the proper SFNM oxidation reaction is set up; using the Mathematic Physics Global ODE and DAEs interfaces, under the section ODE and DAE Interfaces. This step is acquired describing the differential equation:

$$\frac{d(m(t)-m_0)}{dt}\left[\frac{kg}{s}\right] = \iint_{A_{SFNM}} j_{z,CO}(t)\left[\frac{kg}{m^2 s}\right] dA$$

Equation 12 - Differential equation for Carbon Oxide production

Where $j_{z,CO}(t)$ is the carbon monoxide diffusive flux calculated at each time step. It is worth to point out that for Equation 12 is assumed that the variation of mass of the sample during oxidation is only due to CO_2 splitting to CO, without including the formation of other carbon-containing phases in the perovskite. Setting as initial value the null one for the carbon oxide mass existing at that time; while its derivative is calculated solving the equation:

$$\frac{d(m(t)-m_0)}{dt} = (m_{end}-m_0)\frac{d\alpha}{dt}\Big]_{t=0}$$

Equation 13 - Initial ODE condition.

In the Eq.13, all values are known, from the Thermogravimetric analysis data and they are shown in the *Tab. 5*:

Values for the solution of the initial ODE condition

m_{end}	0 [kg]
m_0	6.2622 10^{11} [kg/s]
$\frac{d\alpha}{dt}$	2.5171 10^{-4} [1/s]

Table 5 - Values for the solution of the initial ODE condition.

The condition at the starting time are evidenced in *Tab. 6*:

Initial values for ODE solution (at t= 0 [s])

$m(t) - m_0$	0 [kg]
$\frac{d(m(t) - m_0)}{dt}$	6.2622 10^{11} [kg/s]

Table 6 - Initial values for ODE solution at t= 0 [s]

The reaction is developed and defined, for each reactant, in the Transport of Concentrated Species Physics. In the same Physical section, some conditions, fundamental to describe the passage of the fluid through the porous SFNM; in according to the theory of the diffusion, are inserted.

In terms of thermodynamics parameters, in the modeling, the reaction rate is function only of the temperature, in the Arrhenius equation, there is no partial pressure terms. In addition, concentrations are homogeneous, because of the homogeneity and constancy of the temperature, which doesn't vary in the space and in time, being the process isothermal.

From the second Physics, the third one, Brinkman equations, is defined. The relation, between the porous media and the gas blend, evaluates the problem using a fluid-dynamic point of view; and inserting a Laminar Flow boundary. This phenomenon describes the fluid, which flows from one extreme boundary to the second one, passing though the porous section. The characterization illustrated solves the equations (described in the section 4.2.1 of this work) through the extension of the Darcy's law (Eq. 14) the transitional flow, from the inlet section to the outlet one, the phenomenon is completely portrayed.

$$\varepsilon \vec{u} = -\frac{k}{\mu} \nabla p$$

Equation 14 - Darcy's Law in local form.

4.2.1. Equations

The founding reaction, on which the study will be defined is the Eq. 2.
The reaction is considered as an irreversible process, so, the rate of concentration becomes:

$$\frac{dc_i}{dt} = R_i = \nu_i r$$

Equation 15 - Concentration evolution.

Where:

$$c_i \; is \; the \; concentration \; of \; the \; i^{th} \; species$$
$$R_i \; is \; the \; concentration \; rate \; of \; the \; i^{th} \; species$$
$$\nu_i \; is \; the \; stoichiometric \; coefficient \; of \; the \; i^{th} \; species$$

The reaction rate in the simulation model is calculated as the Eq.4, so it is, also, for the constant rate.

This aspect has to be specified. The physical phenomenon is modelized, also in this section, using the best fitting obtained by the MATLAB simulation, in the previous chapter 3, in the eq. 10.

Input parameters for the calculations in model are represented in *Tab.7*:

SFNM Molecular Weight	*0.40812 kg/mol*
Oxidized SFNM Molecular Weight	*0.42412 kg/mol*
Carbon Monoxide Molecular Weight	*0.02801 kg/mol*
Nitrogen Atomic Weight	*0.014007 kg/mol*
R	*8.3145 J/(mol·K)*
k_0	*14.9 1/s*
E_a	*73500 J/mol*
m_0	*1.6496 10^{-5} kg*
m_{end}	*1.6745 10^{-5} kg*
k_T	$k_0 \, e^{-\frac{\frac{E_a}{R_{gas}}}{773.15\,[K]}} = 1.6127\ 10^{-4}\ 1/s$
Vol_{SFNM}	$\frac{\pi}{4} L_{SFNM} D_{SFNM}^2 (1 - porosity) = 1.131\ 10^{-6}\ m^3$
L_{SFNM}	*0.03 m*
D_{SFNM}	*0.008 m*
L_{CO_2}	*0.135 m*

τ_g	*3*
d_p	*2 10^{-7} m*
Vol	$Vol_{SFNM} + \frac{2\pi}{4} L_{CO_2} D_{SFNM}^2 = 1.4703\ 10^{-5}\ m^3$
ε	*0.25*
μ_{CO_2}	*2 10^{-5} N·s/(m^2)*
Pipe Section	$\pi \frac{D_{SFNM}^2}{4} = 5.0265\ 10^{-5}\ m^2$
$n_{0,SFNM} = n_{CO}$	$\frac{m_0}{Molar\ Weight_{SFNM}} = 4.042\ 10^{-5}\ mol$
m_{CO}	$\frac{n_{CO}}{Molar\ Weight_{CO}} = 1.1322\ 10^{-6}\ kg$

Table 7 - Input COMSOL parameter

The permeability for the SFNM is calculated using the Kozeny-Carman equation:

$$permeability = \varepsilon^2\ \frac{d_p^2}{72\ \tau_g\ (1-\varepsilon)^2} = 2.0576\ 10^{-17}\ [m^2]$$

Equation 16 - Permeability calculation in Model.

For the Transport of Concentrated Species in Porous Media Physics, they will be shown the describing equations of the phenomenon, using the Fick's law for the diffusion:

$$\epsilon_p \rho \frac{\partial \omega_i}{\partial t} + \nabla \cdot \vec{J_i} + \rho(\vec{u} \cdot \nabla)\omega_i = R_i$$

Equation 17 - Describing equation for Transport of Concentrated Species in Porous Media.

Where the Diffusion flux is determined by the expressions:

$$\vec{J_i} = -\left(\rho\ D_i^f \nabla \omega_i + \rho\ D_i^f\ \omega_i \frac{\nabla \left(\sum_i \frac{\omega_i}{MW_i} \right)^{-1}}{\left(\sum_i \frac{\omega_i}{MW_i} \right)^{-1}} \right)$$

Equation 18 - Diffusion flux.

The diffusion coefficients, $D_i^f = 10^{-5}\ m^2/s$.

In the reacting volume, each time step, the production rate, for the carbon monoxide, is calculated as:

$$R_{CO} = r(t)\frac{m_{CO}}{\mathrm{Vol}_{\mathrm{SFNM}}}$$

Equation 19 - Carbon Monoxide production rate.

The Diffusion flux is coupled with the production rate through the Eq.17 to solve the physical diffusion of materials.

For an adequate description of the gaseous flow, the Brinkman equations are used:

$$\frac{1}{\varepsilon_p}\rho\frac{\partial\overrightarrow{u_2}}{\partial t} = \nabla\cdot\left[-p_2\vec{I} + \left(\frac{\mu}{\varepsilon_p}\left[(\nabla\overrightarrow{u_2} + (\nabla\overrightarrow{u_2})^T) - \frac{2}{3}(\nabla\cdot\overrightarrow{u_2})\vec{I}\right]\right)\right] - \left(\mu\kappa^{-1} + \beta\rho|\overrightarrow{u_2}| + \frac{\frac{\partial\varepsilon_p\rho}{\partial t} + \nabla\cdot[-p_2\overrightarrow{u_2}]}{\varepsilon_p^2}\right)\overrightarrow{u_2} + F$$

Equation 20 - Describing equation for the gas flow.

4.2.2. Boundary and initial conditions

The condition at the starting time are showed in this brief subsection.

The initial molar fractions are fixed:

$$\omega_{0,i} = \frac{x_{0,i}MW_{\mathrm{i}}}{\mathrm{MW}_n}\begin{cases} = 0.8_{N_2} \\ = 0_{CO} \\ = 0.2_{CO_2} \end{cases}$$

Equation 21 - Initial molar fraction.

The velocity field is imposed to null, except for the longitudinal component (the z one):

$$\overrightarrow{u_2}\begin{cases} \overrightarrow{u_{2,x}} = 0 \\ \overrightarrow{u_{2,y}} = 0 \\ \overrightarrow{u_{2,z}} = 0.0663\ m/s \end{cases}$$

The extremely low value of the non-null velocity component is determined by the inflow conditions, imposed at the inlet section:

$$Q_{sv} = 200\ cm^3/min = 3.33\ 10^{-6}\ m^3/s$$

The entire microreactor is at the atmospheric pressure: $p_{atm} = 10^5\ [Pa]$.

4.3. Results and optimization

The calculation of the model was carried out until the complete oxidation occurred; the results will be provided as follow.

The reaction is considered concluded when the relative mass variation coefficient reaches the unitary value (*Fig. 27*), as in the model described in the chapter 3.

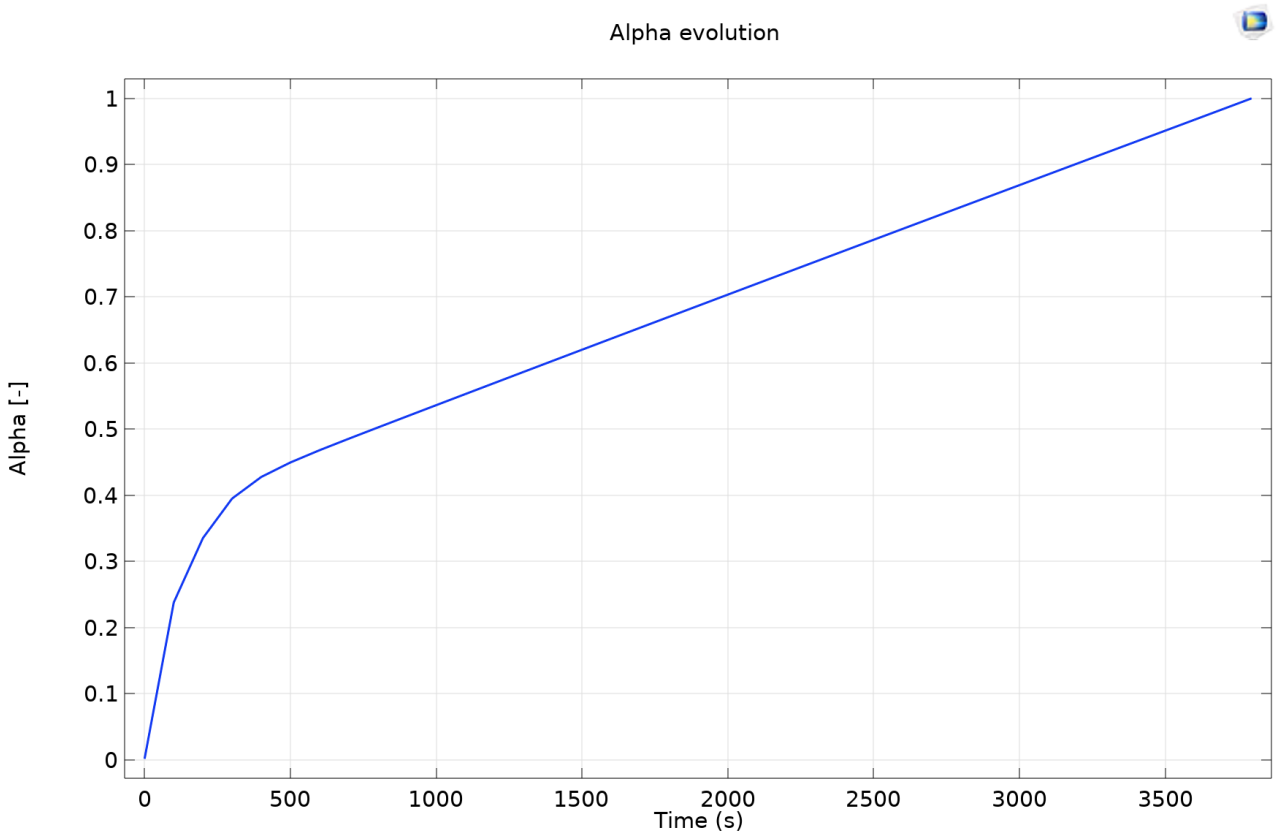

Figure 27 – Normalized mass variation evolution.

The steep increasing in the first 500 s shows that the reaction has a fast kinetic at beginning, i.e. high reacting in that temporal range, followed by a slower and constantly decreasing rate of the reaction.

This expectative is ensured by the following graphs.

In *Fig.28* and in *Fig. 29*, it is illustrated the modelized CO_2 consumption and the coherent CO production during time, in terms of percentage mass in the gas flow.

The relevant observation is given by the initial peak of the two evolutions, this prospect a feasible climax realized by the high reactivity of the material.

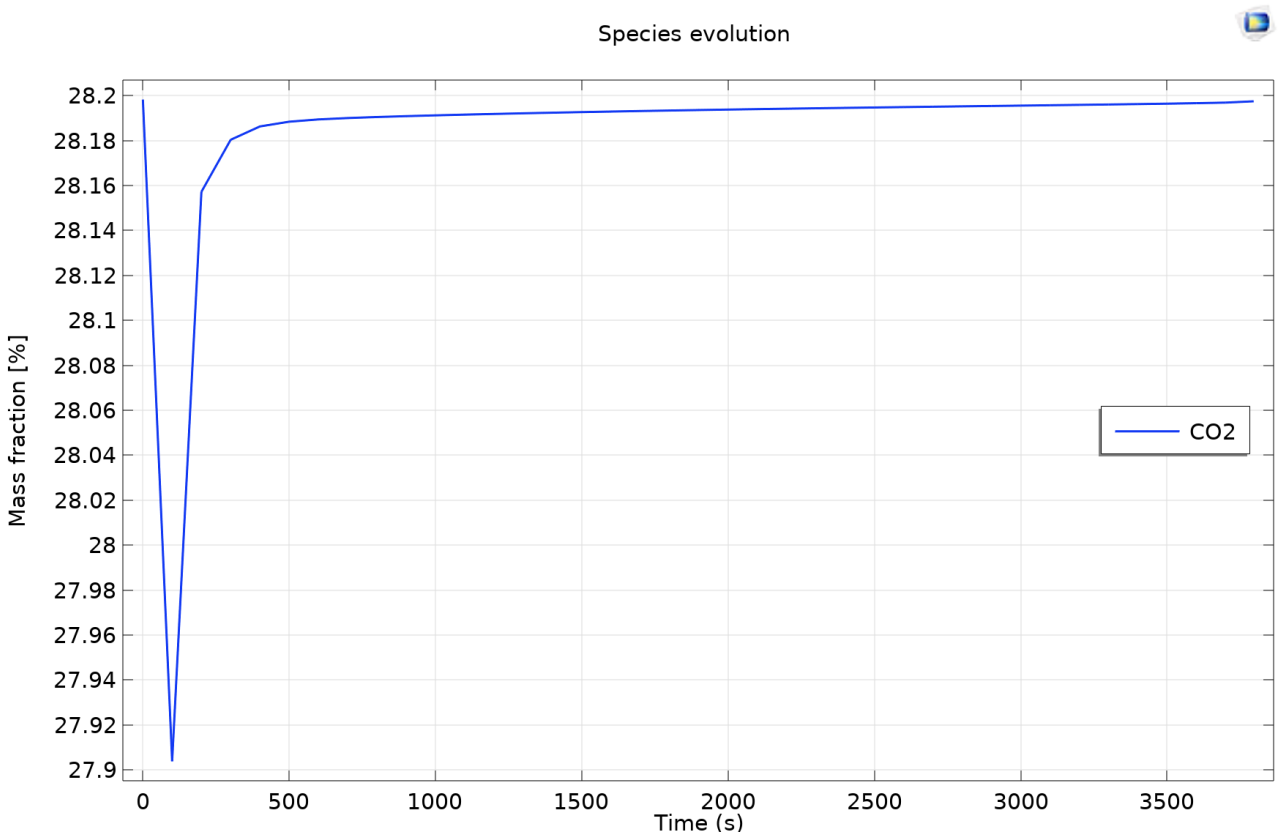

Figure 28 - Concentration evolution for CO_2 consumption.

Subsequent to the drastic drop, the carbon dioxide was not reacting with the material in a significative way, although it was injected in the reactor; so the concentration starts growing, up to the initial value.

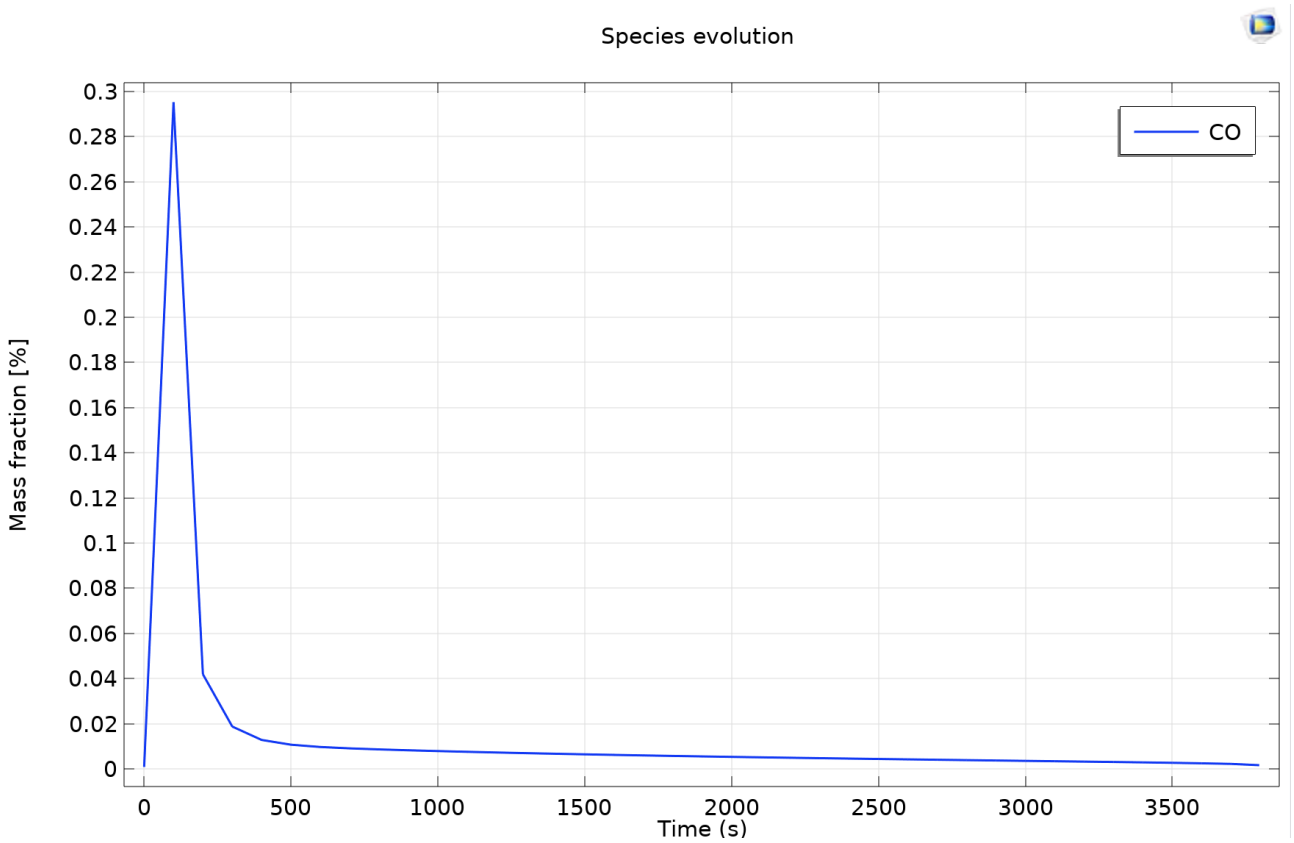

Figure 29 - Concentration evolution for CO production.

Pursuant to the culmination, considering that the gas is not inserted, but rather only produced by the reaction, the CO mass concentration returns to the null value consistently with the CO_2 mass fraction evolution.

The SFNM mass (*Fig. 30*) varying accordingly with the normalized mass variation coefficient, starting from the mass before the oxidation, reaching the greatest value, having obtained the oxygen from the carbon dioxide.

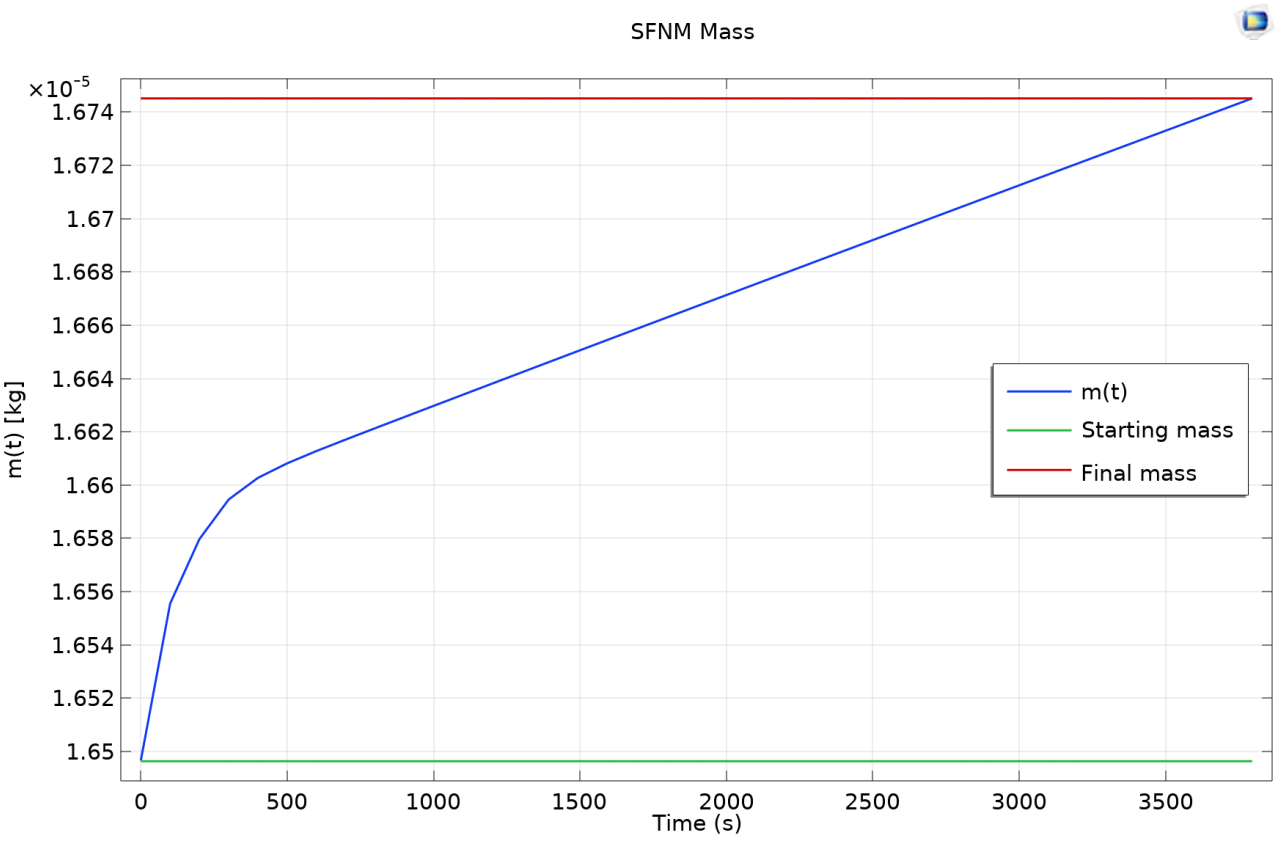

Figure 30 - SFNM mass evolution.

The graphs shows the congruence between the TGA carried out in the chapter 2 and the simulation analysis; entering in the same values range.

The reaction rate, which describes the kinetic behaviour of the reaction is represented in *Fig. 31*:

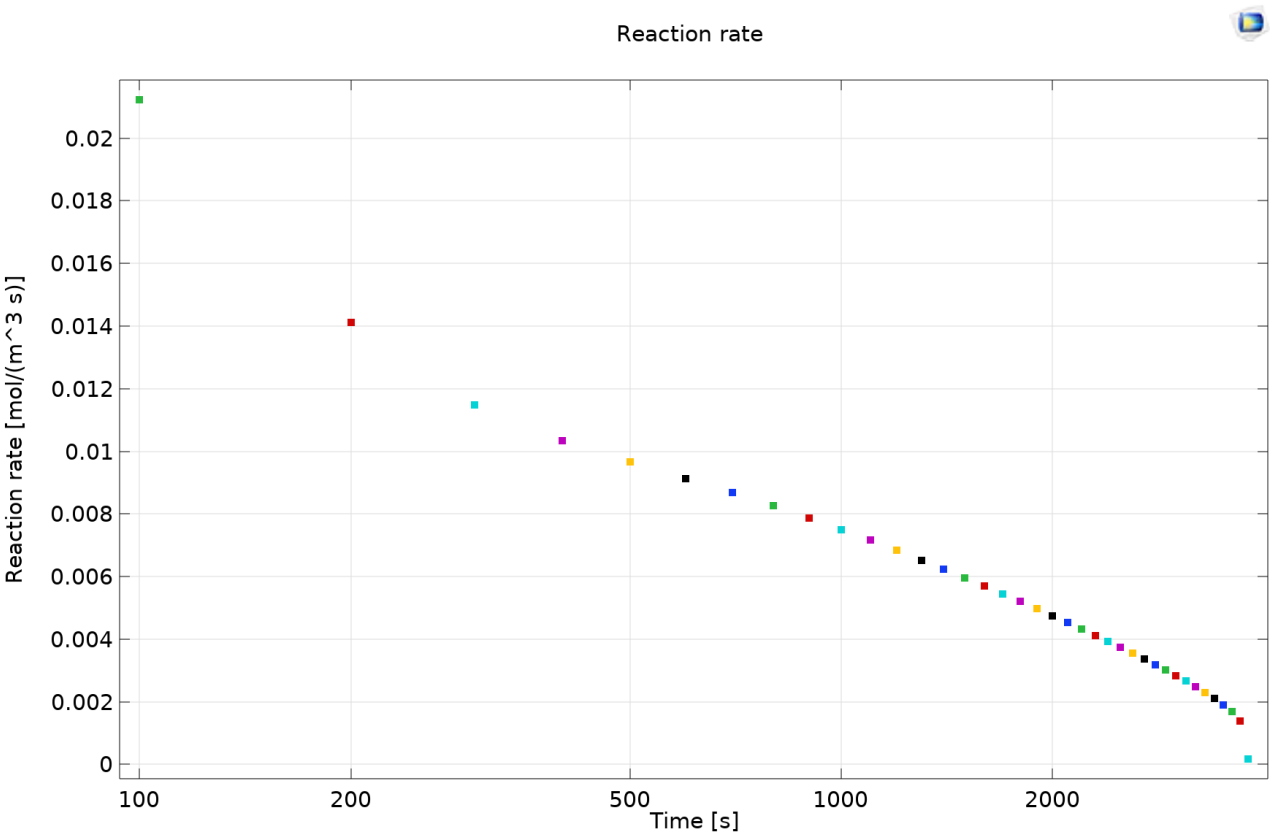

Figure 31 - Rate of reaction evolution, COMSOL (x axis in logarithmic scale).

The plot has a significant value; the maximum of the curve correspond exactly with the high reactivity of the material, in the initial time steps, than, during time, it decrease up to infinitesimal values.
A similar behaviour was found in the model created using the MATLAB script (*Fig. 23*).
These considerations have to be verified in the empirical experimentation, it will be provided in chapter 5.

5. Microreactor validation

The real microreactor testing, applied in the experimental laboratory, is used to validate the model analyzed in previous chapters (3 and 4).

The microreactor used in the laboratory is not properly as the one described in the COMSOL model in the chapter 4, this why real operational conditions give birth to other issues, that in the model could be neglected.

The reactor was composed, initially, by a main pipe, where the SFNM was inserted; this one was rounded by quartz wool, through which the gas was diffusing. This configuration provided results too influenced by systemic errors, during the implementation of the charging of the SFNM.

To abate these errors, due, mainly, to the packing of the sample, it has been decided that the SFNM was inserted inside a smaller crucible, which was directly inserted inside the main pipe.

The new system, composed by a shell inside another shell, reduces, for several factors, the fluctuations of results. The flux of gas invests the Alumina crucible, giving birth to other flows on the walls containing the sample, but this fluid-dynamic phenomenon is not expected to influence results in an huge way.

5.1. Device Description

The outing gas after the microreactor passage was sent to the gas analyzer: Hidden Analytical HPR-20QIC[24] Benchtop Gas Analysis System, which describes the quality, in terms of concentrations of chemical species, of the flow.

Figure 32 - Hiden HPR 20 R&D Benchtop Gas Analysis.

5.2. Experiment

The empirical validation of models, developed in chapters 3 and 4, is carried out developing an oxidation of the SFNM performed by a flow composed, in percentage, by 20% carbon dioxide and 80% of nitrogen; the thermal condition is imposed at 500°C.

The settings of the experiment are the same fixed in the model parameters.

From the first experimental elaboration, described in the chapter 2, fulfilled through the Thermogravimetric device, the maximum CO concentration estimated is low, but with a feasible perspective[24].

As reported in the *Fig. 33*, the production of Carbon monoxide is extremely poor.

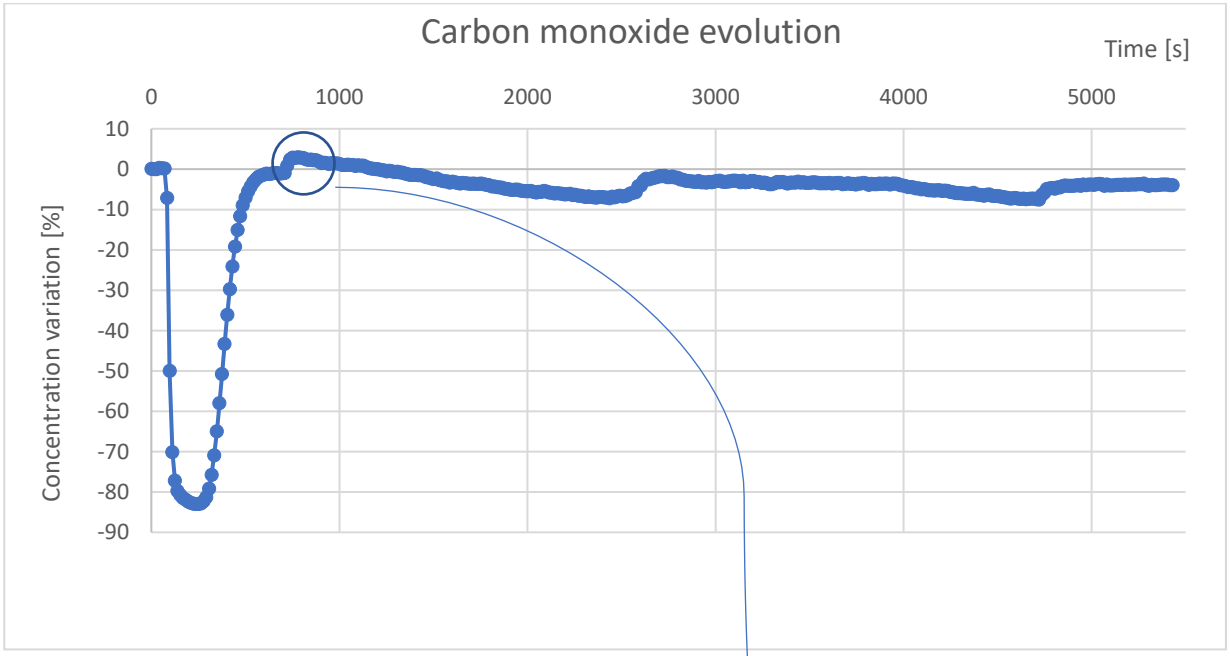

Figure 33 - Carbon monoxide production in Microreactor

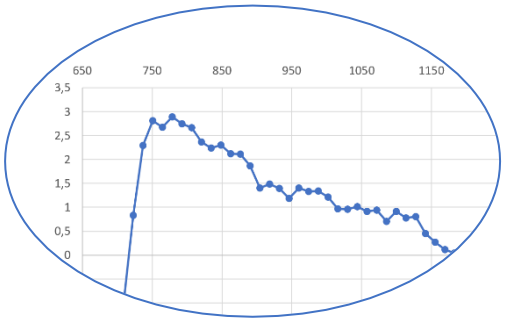

Figure 34 - Carbon monoxide production in Microreactor (zoom view)

The first huge depression is caused by the gas sensor, which has been made undergo by the pressure drop around the valve, later the gas exchange, from the reducing blend to the oxidizing one.
Excluding this explained behaviour, the CO production is almost constant, near the zero. There are, here also, some fluctuations close to the null value, but they are clarified by the tolerance of the gas probe.
On the whole, the production is flat and missing. The only exception is a quick and lacking peak production highlighted in the *Fig. 31*, it persists for 300 s approximately, and it represents, in its highest value around the 3% more than the starting value.
This very low value is not representative for a real concrete validation of the model, because of its not significative evolution and for the range of sensibility of the instrument, whose margin of error fluctuates around the 7%, respect the measure acquired. That positive value, finally, is not consistent because of its low percentage value under the uncertainty threshold. The instrument measure is affected by the variation of the total pressure of gases when feeding the setup with CO_2 using mass-flow controllers, and a system for balancing the inlet pressure of the gases in the mass-spectrometer is needed to avoid the fluctuations in the reading of the CO signal.

6. Conclusion

The work presented has evaluated the kinetic and quantitative estimation of the CO production through the oxidation of the SFNM perovskite using CO_2 in a chemical looping process.

The work started analyzing the material in a Thermogravimetric analysis, which reported some positive perspectives in the results. The potential of the carbon monoxide produced was sufficient. Even if only slightly (0.8% in concentration of the flow produced after the reaction) a potential production of the gas, was observed; inasmuch, the mass of the tested unconventional material was increasing under the effect of the carbon dioxide.

Post mortem analysis, carried out by the department of the Università di Udine, have confirmed the heavy formation of $SrCO_3$ and $SrMoO_4$ on the perovskite surface. This two compounds, generated during the chemical process, make difficult the CO production, performing useless the further oxidation of the material to yield syngas.

The kinetic analysis was carried up in two steps, at first it was performed a code using MATLAB to find the best values for the frequency factor and activation energy; in an iterative way. The results from this step are used in the second step, adopting the numerical simulation of a micro-reactor (COMSOL Multiphysics software), in a more well-structured kinetic model, which takes account the Physics framework too. In this stage, also it is used the definition of the modeling function, suggested as output of the script from the iterative model.

In the second part of the study, the COMSOL simulation provided results which confirm the previous ones emphasizing that the reactivity of the material was significative in the first 500 s seconds of the oxidation, the remaining 90% the reaction occurs with a slow kinetic.

The experimental validation had given no correspondence with respect to the model results. This lack is probably due to the production, in real condition, of other products, which, in first analysis, appeared as carbon monoxide, but, in actual condition, they are not observed.

The huge generation of the strontium carbonate and molybdate during the oxidation represents the main lack of agreement between the model developed and the measured data in microreactor. For this reason, at the end of the dissertation, it can be affirmed that there is no adherence with the results obtained in the chapters 2, 3 and 4. In these sections, it was calculated and modelized the reaction rate for the CO production, which, in the microreactor validation, has been estimated near the zero. This model, at the end of the whole analysis confirm the kinetic behaviour of the $SrCO_3$ and $SrMoO_4$ production, instead of the CO one.

To enhance the kinetic, an increasing of temperature can be applied. Obviously, the rising of the thermal level implicates some loosing of the advantages linked to the SFNM material, respect others already existing in the market.

Another improvement could be applied for the CO_2 percentage supply. If it is intensified, keeping equal the perovskite amount, some upgrades, for the CO production, could occur. Nevertheless, maybe, more $SrCO_3$ and $SrMoO_4$ can arise in a significatively way; absorbing carbon dioxide and not producing the monoxide, useful for the syngas.

In fact, despite the CO_2 seems more productive respect the air oxidation, which is kinetically impulsive, the carbon dioxide's greater yield can be explained by the only outcome of the electrochemical insulators cited far and wide, the $SrCO_3$ and $SrMoO_4$.

Concerning the thermodynamic results linked to this concluding work, the Michigan Institute of Technology are appointed to develop the models. Considering that the kinetic and quantitative analysis have given lacking results, it is suggested to focus their effort on other materials otherwise, on the same SFNM perovskite, but rearranged in view of the results reported in this paper.

One possible change in the analysis can be the used of the water in lieu of the carbon dioxide, producing hydrogen rather than carbon monoxide.

The experimental data are acquired and, although the carbonate and molybdate formation didn't occur, the gas production was not observed.

7. References

1. *https://www.un.org/sustainabledevelopment.*

2. *"International Energy Agency; International Renewable Energy Agency; United Nations Statistics Division; World Bank; World Health Organization. 2020. Tracking SDG 7 : The Energy Progress Report 2020. World Bank, Washington, DC. © World Bank. https://openknowledge.worldbank.org/handle/10986/33822, License: CC BY-NC 3.0 IGO".*

3. *IEA, Energy related CO2 emissions, 1990-2019, IEA, Paris https://www.iea.org/data-and-statistics/charts/energy-related-co2-emissions-1990-2019.*

4. *Portarapillo M., Aronne A., Di Benedetto A., Imparato C., Landi G., Luciani G., 2019, Syngas Production Through H_2O/CO_2 Thermochemical Splitting, Chemical Engineering Transactions, 74, 43-48 DOI:10.3303/CET1974008.*

5. *M. Boaro, A. Felli, "Direct Biopower", PRIN17 Project, University of Udine, 2019-2020.*

6. *A.E. Farooqui, A. Manfredi Pica, P. Marocco, D. Ferrero, A. Lanzini, S. Fiorilli, J. Llorca, M. Santarelli, Assessment of kinetic model for ceria oxidation for chemical-looping CO2 dissociation, Chemical Engineering Journal, Volume 346, 2018, Pages 171-181, ISSN 1385-8947, https://doi.org/10.1016/j.cej.2018.04.041.*

7. *F. Orsini, "Experimental and numerical analysis of thermochemical cycles using cerium oxides and iron oxides", Politecnico di Torino, 2020.*

8. *Hadi Ebrahimi, Mohammad Rahmani, Modeling chemical looping syngas production in a microreactor using perovskite oxygen carriers, International Journal of Hydrogen Energy, Volume 43, Issue 10, 2018, Pages 5231-5248, ISSN 0360-3199,* https://doi.org/10.1016/j.ijhydene.2018.01.108.

9. *Shiqing Hu, Lixiao Zhang, Huanying Liu, Wenping Li, Zhongwei Cao, Lili Cai, Yue Zhu, Xuefeng Zhu, Weishen Yang, Detrimental phase evolution triggered by Ni in perovskite-type cathodes for CO2 electroreduction, Journal of Energy Chemistry, Volume 36, 2019, Pages 87-94, ISSN 2095-4956,* https://doi.org/10.1016/j.jechem.2019.06.001.

10. *O. Das, D. Bhattacharyya, "Durability and Life Prediction in Biocomposites", "Fibre-Reinforced Composites and Hybrid Composites", 2019.*

11. *B. Thorihara Tomoda, M. Agostini de Moraes, "Biopolymer Membranes and Films", 2020.*

12. *S. Ebnesajjad, "Surface Treatment of Materials for Adhesive Bonding", (Second Edition), 2014.*

13. *J. Abraham, S. Thomas, "Phytonanotechnology", 2020.*

14. *J. Abraham, S. Thomas, "Characterization of Nanomaterials", 2018.*

15. *V. Koncar, "Smart Textiles for In Situ Monitoring of Composites", 2019.*

16. *Y. Peng, R. Narain, "Polymer Science and Nanotechnology", 2020.*

17. *S. A. Hashemifard, M. Rezaee, "Synthetic Polymeric Membranes for Advanced Water Treatment", "Gas Separation, and Energy Sustainability", 2020.*

18. *J. Abraham, S. Thomas, "Phytonanotechnology", 2020.*

19. www.netzsch-thermal-analysis.com/it/.

20. *Hou, Limin & Yu, Qingbo & Wang, Kun & Qin, Qin & Wei, Mengqi & Yang, Fan. (2018). Oxidation kinetics of YBaCo4O7+δ and substituted oxygen carriers. Royal Society Open Science. 5.180150.10.1098/rsos.180150.*

21. *Khawam, Ammar, and Flanagan, Douglas R. "Solid-State Kinetic Models: Basics and Mathematical Fundamentals." The Journal of Physical Chemistry. B 110.35 (2006): 17315-7328.*

22. *J. H. Stock, M. W. Watson, "Introduction to econometrics".*

23. www.HidenAnalytical.com

24. M. Dequino, Preliminary redox assessment study on double perovskite structure $Sr_2FeNi_{0.4}Mo_{0.6}O_{6-d}$ by experimental investigation in TGA and microreactor.